DEC 17 1941

VOL. II. No. 10 OCTOBER 1941

# THE ENGINEERS' DIGEST

## REVIEW OF ENGINEERING PROGRESS ABROAD

*PRINCIPAL CONTENTS*

Principles of Design and Selection of Fans and Compressors

Behaviour of Rubber Springs under Variable Loading Conditions

Stressing of Lorry Chassis Frames

Synthetic Rubber for Shaft Packing

Measurement of Photo Recording of Magnetostriction by the Kornezky Method

Hydrogen Content, Solubility, Permeability and its Effect upon Flake Formation in Steel

Stress Cracking caused by Hydrogen and Internal Stressing

Impact Strength of Pre-Stressed Specimens

The Use of Fluorescent Materials for Lighting Purposes

Examination of a Crankshaft after 1 Milliard Revolutions

Design of Mechanisms for Endurance Strength

Substitute Materials in Compass Manufacture

Published by Engineers' Digest Ltd., 120, Wigmore Street, London, W.1
Distribution: E. & F. N. Spon, Ltd., 57, Haymarket, London, S.W.1
Price £2 2 0 per year

# THE ENGINEERS' DIGEST

REVIEW OF ENGINEERING PROGRESS ABROAD

**Published Monthly at 120, Wigmore Street, London, W.1**

*Publishers:* ENGINEERS' DIGEST LTD. - - - Telephone: WELBECK 9357

*Advertisement Dept.* - 120, Wigmore Street, London, W.1
Telephone: Welbeck 9357

*Distribution* - - E. & F. N. SPON, LTD., 57, Haymarket, London, S.W.1
Telephone: Whitehall 1860. Telegrams: Fenspon, Lesquare, London

*Editorial Dept.* - - 120, Wigmore Street, London, W.1
Telephone: Welbeck 9357

**Subscriptions to:** ENGINEERS' DIGEST LTD., 120, Wigmore Street, London, W.1, or E. & F. N. SPON, LTD., 57, Haymarket, London, S.W.1

**Annual Subscription of 12 numbers, £2 2s. Single Copies, 4/6**

**ADVISORY COMMITTEE**

J. F. ALCOCK, B.A., A.M.I.Mech.E.
E. ALTON, D.Eng., A.M.Inst.B.E.
H. H. ASBRIDGE, M.B.E., M.I.Mech.E.
R. W. AYERS, M.I.W.
Col. J. BOWDEN, M.Inst.C.E., M.I.Mech.E.
H. H. BROUGHTON, M.I.Mech.E.
F. BUCKINGHAM, B.Sc., A.M.Inst.C.E., A.M.I.Mech.E., A.M.I.E.E.
T. H. BURNHAM, B.Sc. (Lond.), A.M.I.Mech.E.
J. S. CASWELL, M.Sc., M.I.Mech.E.
G. C. SAFFERY COOPER.
J. DICK, Ph.D., B.Sc., A.M.I.Mech.E.
D. FIFE, M.I.Mech.E.
G. E. FOXWELL, D.Sc. (Lond.), F.Inst.P., F.Inst.F., M.Inst.Gas E.
R. GRIFFITHS, M.Sc.
H. HEYWOOD, Ph.D., M.Sc. (Eng.), A.M.I.Mech.E.
O. HURST, M.Inst.N.A.
Capt. J. S. IRVING, M.I.Mech.E., M.I.A.E., A.F.R.Ae.S., M.S.A.E.
F. C. JOHANSEN, M.Sc. (Eng.), M.I.Mech.E., F.R.Ae.S., M.I.Loco.E.
W. J. KEARTON, D.Eng., M.I.Mech.E., A.M.Inst.N.A
Prof. W. KERR, Ph.D., M.I.Mech.E.
G. V. LOMONOSOFF, Dr.Ing., M.I.Mech.E.
B. J. LYMER, M.I.Mech.E.
D. T. MacIVOR, M.I.Mech.E., M.Cons.E.
W. O. MANNING, F.R.Ae.S.
R. B. MATTHEWS, Wh.Ex., A.M.Inst.C.E., M.I.E.E., F.R.Ae.S.
Prof. A. L. MELLANBY, D.Sc., LL.D., M.I.Mech.E.
J. H. R. RATCLIFF, B.Sc. (Eng., Hons.), M.I.Mech.E.
Col. C. W. D. ROWE.
W. A. SCOBLE, D.Sc., A.R.C.Sc., M.I.Mech.E.
P. W. SEEWER, D.E. (Zurich), M.Inst.C.E., M.I.Mech.E.
Prof. S. PARKER SMITH, D.Sc., M.I.E.E., A.M.Inst.C.E.
C. E. H. VERITY, A.M.Inst.C.E., A.M.I.E.E., A.M.I.Mech.E.
E. G. WALKER, F.C.G.I., B.Sc. (Eng.), M.Inst.C.E., M.I.Mech.E., M.Am.Soc.C.E.
Major F. L. WATSON, M.Inst.C.E., M.I.Mech.E.
G. WATSON, M.Inst.C.E., M.I.Mech.E.
C. H. WOODFIELD, M.I.Mech.E., M.I.Struct.E.
T. WRIGHT, Ph.D., M.Sc.
M. L. YATES, M.Sc.Tech., M.A. (Com.), M.I.Mech.E.

# CONTENTS


AERONAUTICS: *page*

Behaviour of Rubber Springs under Variable Loading Conditions .. .. 388
" *The Engineers' Digest*," *Vol.* 2, *No.* 10, *p.* 388.

ELECTRICAL ENGINEERING:

Wind Motors for the Tropics .. .. .. .. .. .. .. 374
" *The Engineers' Digest*," *Vol.* 2, *No.* 10, *p.* 374.

The Use of Wind Power in Farms of the Soviet Union .. .. .. 374
" *The Engineers' Digest*," *Vol.* 2, *No.* 10, *p.* 374.

Wind Driven Generator to Grandpa's Knob .. .. .. .. .. 376
" *The Engineers' Digest*," *Vol.* 2, *No.* 10, *p.* 376.

Measurement of Photo Recording of Magnetostriction by the Kornezky Method .. .. .. .. .. .. .. .. .. 401
" *The Engineers' Digest*," *Vol.* 2, *No.* 10, *p.* 401.

The Use of Fluorescent Materials for Lighting Purposes .. .. .. 404
" *The Engineers' Digest*," *Vol.* 2, *No.* 10, *p.* 404.

HEATING AND VENTILATING:

Principles of Design and Selection of Fans and Compressors .. .. 366
" *The Engineers' Digest*," *Vol.* 2, *No.* 10, *p.* 366.

MECHANICAL ENGINEERING:

Examination of a Crankshaft after 1 Milliard Revolutions .. .. .. 383
" *The Engineers' Digest*," *Vol.* 2, *No.* 10, *p.* 383.

Design of Mechanisms for Endurance Strength .. .. .. .. 384
" *The Engineers' Digest*," *Vol.* 2, *No.* 10, *p.* 384.

Milling of Light Alloys .. .. .. .. .. .. .. 386
" *The Engineers' Digest*," *Vol.* 2, *No.* 10, *p.* 386.

Stressing of Lorry Chassis Frames .. .. .. .. .. .. 394
" *The Engineers' Digest*," *Vol.* 2, *No.* 10, *p.* 394.

Impact Strength of Pre-Stressed Specimens .. .. .. .. .. 397
" *The Engineers' Digest*," *Vol.* 2, *No.* 10, *p.* 397.

Band Viscosimeter .. .. .. .. .. .. .. .. 405
" *The Engineers' Digest*," *Vol.* 2, *No.* 10, *p.* 405.

METALLURGY:

Hydrogen Content, Solubility, Permeability and its Effect upon Flake Formation in Steel .. .. .. .. .. .. .. .. 379
" *The Engineers' Digest*," *Vol.* 2, *No.* 10, *p.* 379.

Stress Cracking caused by Hydrogen and Internal Stressing .. .. 382
" *The Engineers' Digest*," *Vol.* 2, *No.* 10, *p.* 382.

Toughness of Medium-Carbon Forging Steel .. .. .. .. .. 405
" *The Engineers' Digest*," *Vol.* 2, *No.* 10, *p.* 405.

PLASTICS:

Synthetic Rubber for Shaft Packing .. .. .. .. .. .. 391
" *The Engineers' Digest*," *Vol.* 2, *No.* 10, *p.* 391.

Substitute Materials in Compass Manufacture.. .. .. .. .. 393
" *The Engineers' Digest*," *Vol.* 2, *No.* 10, *p.* 393.

# SOUTH BEND *Precision Lathes*

# 13" Tool Room

## NEW SERIES "S"

The South Bend Underneath Belt Motor Drive is the most efficient and practical direct drive equipment for a back-geared screw cutting lathe. This fully enclosed drive is unusually compact and powerful, and is silent and economical in operation.

UNDERNEATH MOTOR DRIVE

BACK-GEARED

QUICK CHANGE GEAR EQUIPMENT

1 H.P. MOTOR

# Buck & Hickman Ltd.

**WHITECHAPEL ROAD LONDON, E.1.**

# EDITORIAL

*Increasing expenditure and thought continue to be devoted to the welfare requirements of workers—and rightly so. It has no longer to be argued that good food, better ventilation, recreational facilities and other amenities adding to the general welfare of the staff are in themselves a direct contribution to increased production and efficiency. But how many firms have diverted a fraction of this expenditure to a Works Library ? What is done to encourage greater knowledge of the technology of their work among the workers themselves ? Here unhappily the story is not the same. Industry to-day tends to inherit in totally different circumstances in its outlook on educational matters some of the old family craftsman characteristics of the last century, when a man took pride in the fact that his craft was acquired at his father's elbow and had been handed down from generation to generation. To-day the position is a vastly different one indeed. Some firms, it is true, have to their credit realized that, although their work is on a mass production basis, intelligence, individualism, skill and efficiency have ultimately to be learned from books alone. A good and up-to-date Works Library is a great asset to any Works. Indeed, some of the largest manufacturers have libraries of which they are justly proud, and they do not hide the fact that they find it in their own interests to maintain them. By attracting the most intelligent and ambitious workers, a Works Library is giving inspiration and help to just those men who are and will continue to be the men of greatest value to the Management. Industry advertises goods it can no longer supply to the trade. Why ? Because they have the foresight to realize that they will need their goodwill when the war is over. Similarly, a firm that establishes a Works Library now derives more than immediate benefit ; it is developing the knowledge and adaptability in its production and factory staffs that will be of the utmost value when once again the wheels are turned over to peace time, with its—who knows how great ?—new technical problems and developments.*

*Books contain often the accumulated experience and knowledge of a life-time, the results of patient experiment bought at great cost. For a few pounds this valuable information can be on your bookshelf, handy, always ready for reference, whether concerning day to day problems or new schemes of far reaching consequence.*

THE ENGINEERS' DIGEST *itself exists to widen the knowledge of the technical staff. Its whole purpose is to provide information of high authority collected from the most expert sources. To complete its object it has decided to provide a further service that is wholly or in keeping with—is indeed inseparable from its avowed objects. It now offers every reader a free Enquiry Service in connection with the best technical books.*

*If you agree that a Works Library will add to the efficiency of your organization, first send to us for our suggestions. We will compile a carefully selected list of books, appropriate to your particular work to the value of the approximate amount which you are prepared to spend. Arrangements can later be made for the books to be obtained through our Book Department, and thus you are relieved of any complications and difficulties. Two hundred pounds would be ample, and in some cases more than ample, to equip a good library, and an annual grant of, say, twenty-five pounds sufficient to keep it up to date. One firm who, with wisdom and foresight, had some years ago installed a library on a moderate scale, had found it contributed so much to the efficiency of their business that, within two days of its destruction by enemy action, they had sent out to publishers an urgent call for catalogues to enable them to replace it as quickly as possible. This indeed is high testimony to what is too often regarded as a side-line, but which is in fact, as the experience of this firm proves, a rich and productive part of the organization.*

# PRINCIPLES OF DESIGN AND SELECTION OF FANS AND COMPRESSORS

By Prof. Dr. Ing. Mario Medici. (From *L'Energia Termica*, Vol. 8, No. 3, March, 1940, pp. 50-69).

The introduction of a general parameter of reference which gives an exact picture of the design of compressors in respect of their three fundamental characteristics, namely compression ratio, volumetric output and speed, makes it possible to select the most suitable type of machine for the conditions of service. Further, it gives some useful indication how to plan programmes for economic production, and how to record the results of tests.

The specific speed of compressors is given by:

$$n_s = n \cdot V^{0.5} \left( \frac{\Delta p}{\gamma/g} \right)^{-0.75} \quad \ldots \quad \ldots \quad \ldots \quad (1)$$

where $\gamma$ is the density of the fluid, V is the output in m³/sec. and $\Delta p$ is the pressure head impressed in mm. water gauge by the machine on the fluid. This expression can be written in a more convenient form by introducing the dimensions $D_G$ and $D_M$ the outer and inner diameter of the rotor of axial flow compressors, and $D_2$ and $D_1$ for radial flow impellers respectively. The application of the laws of proportionality gives the two equations

$$\Delta p = \Psi \cdot \gamma \cdot \frac{u_2^2}{2g} \quad \ldots \quad \ldots \quad (2), \text{ and}$$

$$\left.\begin{aligned} V &= \psi \frac{\pi}{4}(D_G^2 - D_M^2)u_2 \quad \text{for axial flow type} \\ V &= \psi \frac{\pi}{4} D_2^2 \, u_2 \quad \text{for radial flow type} \end{aligned}\right\} (3)$$

Substituting these values into equation (1), we obtain

$$\left.\begin{aligned} n_s &\propto \psi^{0.5} \cdot \Psi^{-0.75} \left[ 1 - \left( \frac{D_M}{D_G} \right)^2 \right]^{0.5} \text{ for axial flow type} \\ n_s &\propto \psi^{0.5} \cdot \Psi^{-0.75} \text{ for radial flow type} \end{aligned}\right\} (4)$$

Besides these two coefficients, $\Psi$ and $\psi$, a power coefficient $\lambda$ has been proposed by Berlowitz and has been adopted in German practice for testing centrifugal compressors. According to B. Eck, $\lambda$ takes the form:

$$\lambda = \frac{P_a}{\gamma/2g \cdot u_2^3 \cdot \frac{\pi D_2^2}{4}} \quad \ldots \quad \ldots \quad \ldots \quad (5)$$

Where $P_a$ is the power imput on the shaft in kgm/sec., $D_2$ the outer diam. of blading in m, and $u_2$ the circumferential velocity in m/sec. corresponding to $D_2$.

The consideration of $\lambda$ is useful for estimating the losses of the machine at zero output, and for specifying the characteristics of the driving motor with regard to the maximum power required.

## Radial Flow Fans.

Considering a cylindrical section, the difference of pressure between the pressure side and aspiration side of each vane is given by:

$$dp = \frac{\gamma}{2g} (w_t^2 - w_f^2)$$

where $w_t$ and $w_f$ are the relative velocities of flow at the two sides of the vane (Fig. 2). Provided the flow between the blades is continuous, without zones of stagnation and cavitation, the law of

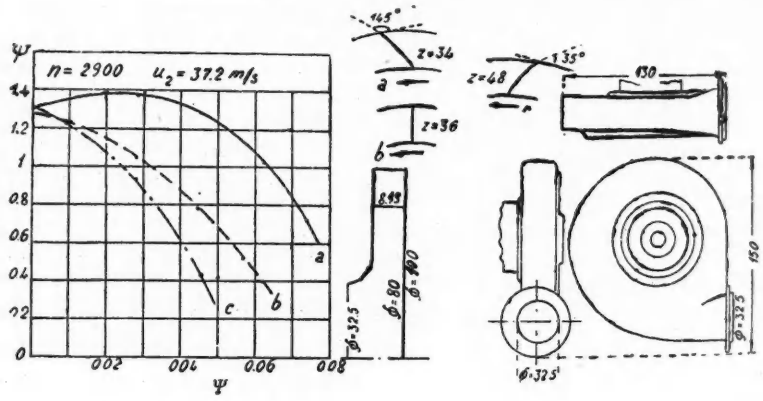


Fig. 1
Characteristics of a Meidinger type radial fan (experiments with different bladings).

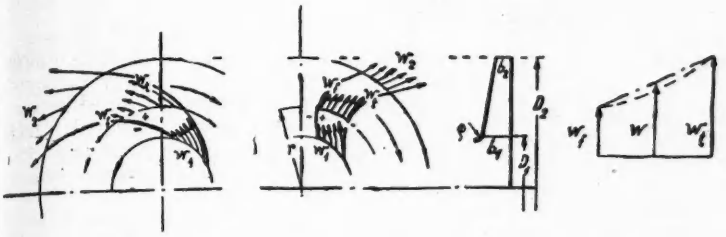

Fig. 2
Distribution of the relative velocity W along the rotor of a radial fan.

variation of the relative velocity is intermediary between a curvilinear and a straight-line law. This condition may be fulfilled, at normal output, with convex bladings ($\beta_{2c}$ from 35 to 70°) or with concave bladings ($\beta_{2c}$=125 to 155°). (See Fig. 3).

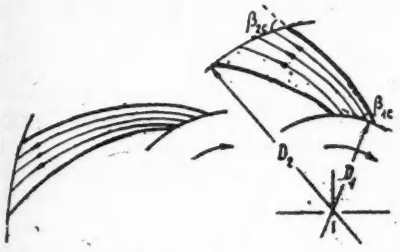

Fig. 3. Flow-lines in a rotor blading.

The constant velocity w along the blading is also of fundamental importance for the *aero-dynamic* behaviour of the rotor. Constancy of the relative velocity from the inlet to the outlet increases the *aero-dynamic* efficiency. With radial flow compressors this can be achieved with either convex blades ($\beta_{2c} \leqq 70°$) or concave blades ($\beta_{2c}$ from 125 to 145°). Making $\beta_{2c} = 90°$ is therefore, not justified.

With a pluri-dimensional consideration of the flow, the theoretical amount of the pressure increase $\Delta_{pt}$ may be determined by a mixed analytical-graphical method (Fig. 4), the values of $w_t$ and $w_f$ being plotted against the developed length of the blades. The values of dp.b.R are calculated, where b=axial width of the vane, R= radius of the cylinder considered. Hence:

$$| \Delta P |_t = \frac{M.\omega}{V} = \frac{\omega.z}{V} \int_{R_1}^{R_2} dp \cdot b \cdot R \cdot dR \ldots (6)$$

where z= the number of blades.

The ratio $i = | \Delta P |_t / | \Delta P |_E$ * indicates the theoretical diminution of the power output for the industrial wheel with a definite number of blades, compared with the ideal wheel, with an infinite number of blades. This diminution ranges from 20 to 25% for concave blading and only about 13 to 15% for convex blading, since the tendency to form zones of stagnation is more pronounced in the case of the former. This diminution of the theoretical power includes a reduction of the K.E. of the flow leaving the wheel, and a corresponding increase of the reaction, and should be regarded as advantageous as the efficiency of diffusers or volute casings is moderate.

* $| \Delta P |_E = \frac{\gamma}{2g} [ (u_2^2 - u_1^2) + (c_2^2 - c_1^2) + (w_2^2 - w_1^2) ]$

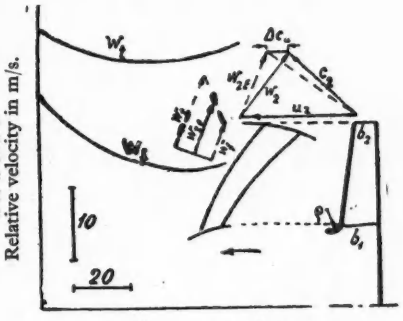


Fig. 4
Determination of the relative velocities $W_t$ and $W_f$ along the flow passing through the rotor blading.

Developments of blades in mm.

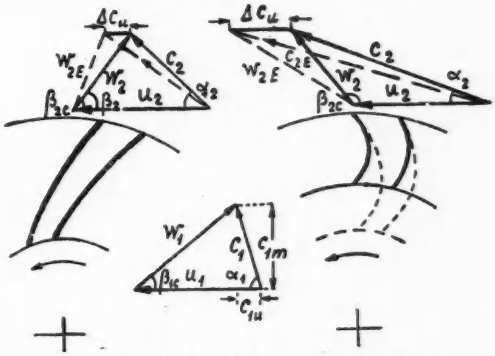

Fig. 5. Velocity diagrams of different vanes.

**The Energy Losses.**

The transformation of the fluid in compressors without cooling arrangements is a polytropic process according to the equation

$$q_{pol}=c_p(T_f-T_i) \quad .. \quad .. \quad .. \quad (7)$$

where $T_f$ and $T_i$ are the fluid temperatures at the end and at the beginning of the transformation respectively, $q_{pol}$ = heat in Cal/kg, $c_p$ = sp. heat at constant pressure in Cal/kg. By a comparison with the corresponding adiabatic transformation:

$$q_{ad}=c_p(T_{f\cdot ad}-T_i) \quad .. \quad .. \quad (8)$$

we obtain the adiabatic or internal efficiency of the compressor

$$\eta_{tf}=\frac{T_{f\cdot ad}-T_i}{T_f-T_i} \quad .. \quad .. \quad .. \quad (9)$$

The calorimetric determination of this efficiency is very simple, if we neglect the natural refrigeration effect of the exterior casing surface. $T_f$ and $T_i$ can be measured directly by thermometers, and $T_{f\cdot ad}$ can be calculated from

$$T_{f\cdot ad}=(T_i+273)\left[\frac{P_f}{P_i}\right]^{\frac{k-1}{k}} \quad .. \quad .. \quad (10)$$

The gross or industrial efficiency, denoted by $\eta$, includes the adiabatic efficiency $\eta_{tf}$, the volumetric efficiency $\eta_v$, the mechanical efficiency $\eta_m$, and the ratio of power $P_f$ (in KW) *dissipated* by friction between the rotor and the fluid, and the utile power $P_u$ (in Kw.). Thus:

$$\eta=\frac{1}{\frac{1}{\eta_{tf}}\cdot\frac{1}{\eta_v}+\frac{1}{\eta}-\frac{1}{\eta}\left[\eta_m+\frac{P_f}{P_u}\right]} \quad .. \quad (11)$$

For the evaluation of volumetric losses it is useful to refer to diagrams like Fig. 6, which indicates the ratio between the volumetric losses through the clearances and the utile output ($V_f/V$) for different values of the diameter ratio ($D_2/D_1$). (m) represents a curve for average accuracy, and that of (g) for more rough executions. The volumetric efficiency is given by

$$\eta_v=\frac{1}{1+\frac{V_f}{V}} \quad .. \quad .. \quad .. \quad (12)$$

The mechanical losses arise from friction on bearing surfaces. In general they are only of modest percentage.

For the evaluation of the power dissipated by friction between the rotor and the fluid, reference should be made to Fig. 7. The values of $P_f/P_u$ are given as a function of $b_2/D_2$ with different values of $C_{2m}/u_2$ and of $\Psi$ as parameters. This diagram shows that these losses are relatively small, with values between 2 and 3% for $b_2/D_2$ = 0.12, which is a very low value indeed for radial flow fans.

The factors affecting the internal efficiency of the compressors are the losses by friction in the rotor and in the casing ($\Delta p_a$), the losses by cavitation of the flow in the rotor and along the casing ($\Delta p_d$), the losses by sudden deflection ($\Delta p_{bd}$), and the losses due to diffusion operations ($\Delta p_{tr}$). Therefore the internal efficiency may be expressed as

$$\eta_{tf}=\frac{\eta}{\eta_m-\frac{P_m}{P_u}\eta}\cdot\frac{1}{\eta_v}=\frac{\Delta p}{\Delta p+\Delta p_a+\Delta p_d+\Delta p_{bd}+\Delta p_t} \quad .. \quad .. \quad (13)$$

For a given specific speed of a fan, the conditions for minimum losses may be determined by differentiation from which the optimum value of $\Psi$ may be deduced. Hence

$$\psi_{opt}=\text{const}\cdot\left[\frac{|\,c_2\,u\,|_E}{u_2}\right]^6$$

where the constant is a sixth degree function of the diminution index (i). In the first approximation we obtain

$$\psi_{opt}=1{\cdot}5\left[\frac{|\,c_2\,u\,|_E}{u_2}\right]^6 \quad \text{for convex blades} \quad (\beta_{2c}<90^\circ)$$

$$\psi_{opt}=0{\cdot}75\left[\frac{|\,c_2\,u\,|_E}{u_2}\right]^6 \quad \text{for concave blades} \quad (\beta_{2c}>90^\circ).$$

At normal output the losses due to friction and diffusion are predominant over other losses. For a given casing and configuration of the diffuser guide vanes, the losses by diffusion are in proportion to those by friction. Therefore it is sufficient to establish the condition for the minimum of frictional losses.

The deviation of the flow at the wheel inlet requires a generous radius of curvature and continuous acceleration of the flow at this point, in order to avoid the phenomenon of cavitation in the more straight zones of the inlet bend.

It is necessary to fulfil the condition

$$\frac{\pi}{4}D_1^2=\epsilon\,\pi\,D_1\,b_1 \quad .. \quad .. \quad (14)$$

where $\epsilon$ is a coefficient of majoration which increases when the minimum radius of curvature decreases. A good value for $\epsilon$ is 1.2.

The thickness of the blades reduces the space available for the flow. We have:

$$C_{1m}=C_{0m}\left[\frac{t}{t-\frac{s}{\sin\beta_{1c}}}\right] \quad .. \quad .. \quad (15)$$

where (t) is the blading pitch and (s) the thickness of the blades.

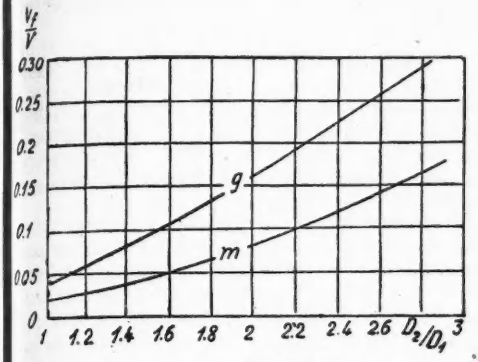


Fig. 6. Percentual values of the clearance losses plotted against the ratio of the blading diameter.

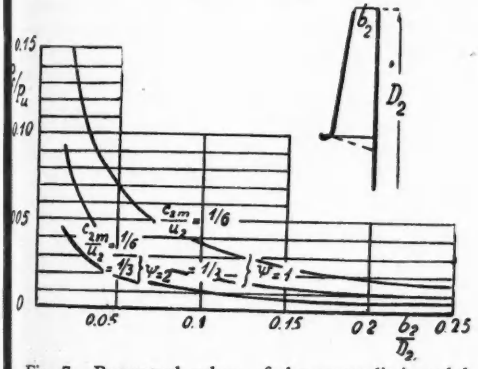


Fig. 7. Percentual values of the power dissipated by friction between the medium (air or gas), and the rotor.

From the velocity diagram at the inlet (Fig. 5) we get :

$$w^2=u_1^2+C_{1m}^2=\left[u_2\frac{D_1}{D_2}\right]^2+\left[\frac{V}{\pi D_1 b_1}\cdot\frac{t}{t-\frac{s}{\sin\beta_{1c}}}\right]^2 \quad (16)$$

which can be expressed as

$$w^2=u_2^2\left(\frac{D_1}{D_2}\right)^2+\left\{\frac{u_2\psi\epsilon}{(D_1/D_2)^2}\left[\frac{t}{t-\frac{s}{\sin\beta_{1c}}}\right]\cdot\left[1-\left(\frac{d}{D_1}\right)^2\right]\right\}^2 \quad (17)$$

where (d) is the hub diameter or the shaft diameter. By differentiation and equating to zero we obtain the condition for a minimum and we arrive to

$$\frac{D_2}{D_1}=\frac{1}{\sqrt[3]{\sqrt{2}\cdot\epsilon\cdot\psi\left[\frac{t}{t-\frac{s}{\sin\beta_{1c}}}\right]\cdot\left[1-\left(\frac{d}{D_1}\right)^2\right]}} \quad (18)$$

From the above equation, the values of $u_1=u_2\,D_1/D_2$ and $c_{1m}$ can be determined, from which $|\beta_1|_{opt}$ was found to be 35°. Similarly the optimum value for the inlet diameter of the rotor $D_1$ can be found. Modifying $D_1$ increases the average inlet velocity of the flow as shown in Fig. 8a. The curve shown there is defined by $C_1 u_1^2 = \text{const}$. Therefore, if $D_1$ diminishes, $u_1$ decreases too, but $C_1$ increases; on the other hand if $D_1$ increases beyond $D_{1\text{-opt.}}$, $u_1$ increases but $C_1$ decreases. Therefore an increase of $w_1$ beyond $w_{1\ min}$ cannot be avoided.

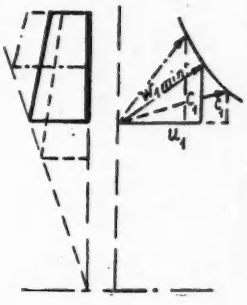


Fig. 8a

Recently B. Eck has indicated the effect of divergencies between the actual values and the optimum values of both, $D_1$ and $\beta_1$, on the behaviour of the machine. By determining the numerical values of $(W_1/W_{t\text{-opt}})^2$, he found that in order to keep this lower than 1.035, $\beta_{1c}$ should have values between 28° and 44°.

The most advantageous value of the axial height of the rotor at the inlet is deduced from the equation (14) and is given by

$$|b_1|_{opt}=\frac{D_1}{4\epsilon} \quad \ldots \quad (19)$$

This depends upon the inlet diameter $D_1$, and the acceleration estimated to be impressed on the flow at the wheel inlet. But this acceleration is not sufficient to avoid cavitation if it is not accompanied by a sufficient filleting of the lateral rotor walls. The variation of the meridianal velocity $c_{1m}$ (Fig. 8b) along $b_1$

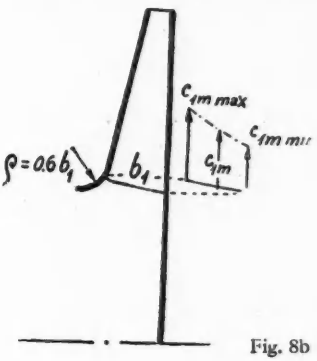


Fig. 8b

must not exceed certain limits, if the efficiency is not to suffer. The ratio $|C_{1m}|_{max}/|C_{1m}|_{min}$ is an index of the mentioned velocity variation and of the super-position of transversal movements over the principal flow. From calculated values of $b_1/\rho$ as a function of the mentioned ratio, it was found that it is advisable to keep $\rho \geq 0.6b_1$ ($\rho$ is the minimum radius of curvature). Because of the limited radial development of the blades, especially with drum rotors, it is good practice to subdivide the blading zone as shown in Fig. 9.

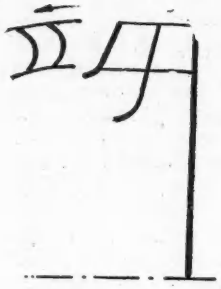

Fig. 9

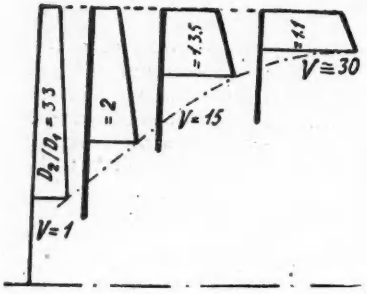


Variations of the form and dimensions of the rotor of radial fans according to the variation of the ratio $D_2/D_1$ (for the same $U_2$ and $D_2$).

Fig. 10

**Application of Fans in the Modern Industry.**

The application of radial flow covers a field with the ratio $D_2/D_1$ varying between 3.3 and 1.1, with a corresponding variation of output between V=1 and V = 30.m³/sec.

Drum runner type fans require a larger number of blades to give the flow sufficient guiding, and concave blades are used with outlet angles between 125° and 140°.

In proportion to the decrease of the ratio $D_2/D_1$ for drum runners, the ratio $b_2/D_2$, and the susceptibility to the phenomenon of reflexion on the side walls increases. Improvements can be obtained by using conical runners or side walls, or by using intermediate screens. It is good practice to use a blade pitch of $0.7r < t < r$ for drum runners, where (r) denotes the radius of curvature of the blades. The number of blades varies between 125 and 44, with $D_2/D_1$ varying between 1.1 and 1.25. The ratio most frequently used in modern industrial design is $D_2/D_1=1.14$, with a corresponding number of blades, z=75 to 105.

To obtain the best *aero-dynamic* conditions it is advisable to satisfy the condition

$$\sin(180°-\beta_2)=\sin\beta_1\frac{D_1}{D_2}\cdot\frac{b_1}{b_2} \quad .. \quad (20)$$

for continuity of flow. This indicates that for runners with parallel walls, $(180-\beta_2)$ is always less than $\beta_1$, ($b_1=b_2$ in this case). The adoption of conical runners leads to a compensation between $D_1/D_2$ and $b_1/b_2$.

A comparison between radial and drum type fans will show that the coefficients $\psi$ and $\Psi$ are much higher for the latter type, for equal values of V, $\Delta$ p and n. The reduction of size and cost resulting from the adoption of drum runners while (n) remains the same is obvious. It is, however, advisable to adopt smaller speeds for this type of fan, since the losses due to sudden deviation of the flow for outputs other than that corresponding to the minimum of the said losses, are inversely proportional to the pressure coefficient $\Psi$.

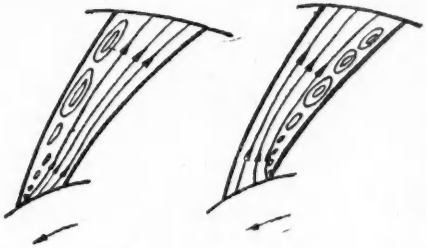

Fig. 11. Cavitation of the flow on the surface under depression (at reduced outputs), and on the surface under pressure (at increased outputs).

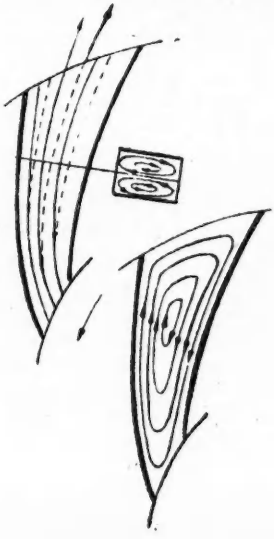

Fig. 12

Effect of the superposition of a double transversal vortex on the principal flow in the rotating system. (The plain lines show the stream-lines in the centre of the orifices), the interrupted lines show them near the lateral walls of the rotor.

**Losses by Sudden Deviation of Flow and Cavitation.**

At outputs other than normal, additional losses appear owing to sudden deviation of the flow at the inlet of the blading, and cavitation of flow may also occur (Fig. 11). As a result of the latter phenomenon a double transversal vortex is, generally, superimposed on the principal flow through the blading (Fig. 12). This circumstance indicates a difference of behaviour at different cross-sections and hence the necessity of a three-dimensional consideration of the flow, if an exact evaluation of the theoretical output is required.

The examination of the pressure coefficient $\Psi$ gives some information about the losses. The losses of energy transformation increase directly with $\Psi$, and an increase of $\Psi$ can be avoided only if the diffusion arrangements are carefully designed.

**Dimensioning.**

Usually, the values of $\Delta$ p and V are fixed; also the value of (n) is frequently specified. In this case, the specific speed is given and the value of $\Psi$ can be determined. The category and general design of the fan may be now fixed; as a guide the following should be noted:

for $\Psi = 0.7 \longrightarrow 1.25$, runner with convex vanes should be adopted

for $\Psi = 1.25 \longrightarrow 2.25$, drum runner should be adopted.

From $\Psi$ the circumferential velocity may be calculated:

$$u_2 = \sqrt{\frac{2g \cdot \Delta p}{\gamma \cdot \Psi}} \quad .. \quad .. \quad (21)$$

and the rotor outlet diameter

$$D_2 = \frac{60\, u_2}{\pi \cdot n} \quad .. \quad .. \quad .. \quad (22)$$

and further

$$\psi = \frac{4V}{\pi D_2^2 u_2} \quad .. \quad .. \quad .. \quad (23)$$

After the acceleration of the flow at the runner inlet is fixed ($\epsilon$), the radial runners may be designed by estimating to the first approximation, the values of

$$\frac{t}{t - \frac{s}{\sin \beta_{1c}}} \quad \text{and} \quad \left[1 - \left(\frac{d}{D_1}\right)^2\right]$$

and hence the optimum inlet diameter may be calculated: $|D_1|_{opt} =$

$$\frac{D_2}{\sqrt{\sqrt{2} \cdot \psi \cdot \epsilon \cdot \left[\frac{t}{t - \frac{s}{\sin \beta_{1c}}}\right] \cdot \left[1 - \left(\frac{d}{D_1}\right)^2\right]}} \quad (24)$$

from which the axial length at the inlet can be found:

$$|b_1|_{opt} = \frac{D_1}{4\epsilon} \quad .. \quad .. \quad .. \quad (25)$$

With these elements and an appropriate choice of z and $b_2$, the wheel and its blading may be designed. Some corrections of the previously calculated values may become necessary and, therefore, a repetition of the whole calculation with the new values takes place. Next the output reduction coefficient (i) will be determined, by calculating $\Delta$ $p_E$ from Euler's* equation and $\Delta$ $p_t$ from equation (6). The velocity triangles can now be drawn, and the diffuser guide vanes designed.

The approximate value of the internal efficiency is determined from values assumed for the different losses, and the total efficiency is deduced by considering diagrams (6) and (7). This may necessitate some corrections of the previously executed calculations.

For drum rotors the value of $D_1$ can be obtained from considering the best value for $D_2/D_1$. Thence the ratio $b_2/b_1$ is determined. It is advisable to make $b_1 = 0.25$ to $0.22\ D_1$.

If the speed is not fixed, dimensioning proceeds in a similar manner except that values for both $\psi$ and $\Psi$ will be assumed. Then to the first approximation

$$\frac{D_2}{D_1} \backsimeq \frac{0{\cdot}84}{\sqrt[3]{\Psi}} \quad .. \quad .. \quad (26)$$

As $u_2$ is given by

$$u_2 = \sqrt{\frac{2g \cdot \Delta p}{\gamma \cdot \Psi}} \quad .. \quad .. \quad (27)$$

$D_2$, n and $D_1$ can be calculated.

The velocity at the fan entrance should be, for both radial and airscrew fans,

$$C_A = k \sqrt{\frac{\Delta p}{\gamma}} \quad .. \quad .. \quad (28)$$

where k is a constant having a value of 0.85 for high pressure fans and 1.8 for low pressure fans. (k seems to have rather divergent values).

**Axial Flow Fans.**

Axial flow fans have propeller rotors and tubular casings, in general of the convergent-divergent shape. It is an established fact that better results can be obtained if a pre-distributor is followed by the impeller (Fig. 13a), than if the impeller is followed by a diffuser combined with guides (Fig. 13b).

*Euler's Fundamental Equation:

$$|\Delta p|_E = \frac{\gamma}{2g}[(u_2^2 - u_1^2) + (c_2^2 - c_1^2) + (w_2^2 - w_1^2)]$$

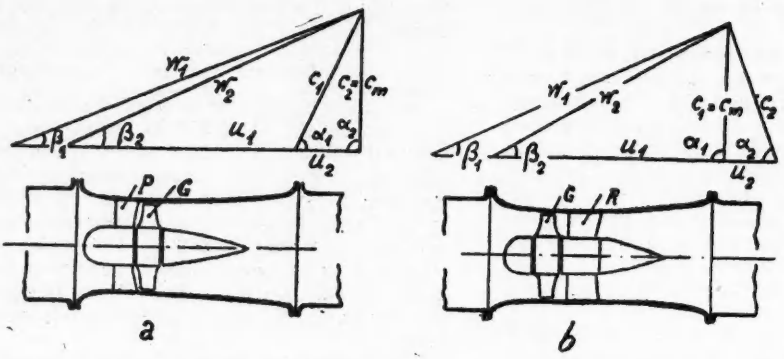


Fig. 13.

Axial fans with air-screw-type impellers: (a) Guides before the impeller; (b) Impeller followed by a rectifier-diffuser.

The chief advantages attached to this type of fan are: smaller dimensions and weight, with consequently reduced costs, and easier and better connection into the ventilation plant. On the other hand, the attendant disadvantages are: lower pressure obtainable for a given circumferential speed, increased wear, especially in the case of a gas with dust in suspension, and noisier working.

**Aero-Dynamic Considerations about Propeller Type Fans.**

For the aero-dynamic analysis of axial flow fans, it is customary to assume that the stream lines representing the principal flow are disposed on concentric surfaces. It is sufficient to consider an adequate number of coaxial cylinders developed each on a plane. The three-dimensional flow can be thus analysed by the consideration of a number of two-dimensional flows. This disposition of the profiles involves two aero-dynamic facts:

(1) The blade profiles are in a slightly curved stream-line flow.

(2) Although the blade thickness and friction produces acceleration of the mean velocity of flow (owing to restriction of space), the flow has a de-acceleration.

The aero-dynamic action has two components: One perpendicular to the flow (S) represents the lift, and the other in the direction of flow (R) representing the drag. The analytical expression deduced for S and R for a cylindrical section of the propeller, having a radial height R, are

$$\left.\begin{aligned} S &= |C_p|_s \frac{\gamma}{2g} \cdot \Delta R \cdot l \cdot w_\infty^2 \\ R &= |C_R|_s \frac{\gamma}{2g} \cdot \Delta R \cdot l \cdot w_\infty^2 \end{aligned}\right\} \quad .. \quad (29)$$

where $w_\infty$ = relative velocity of the non-disturbed flow, $l$ is the length of the chord of the blade profiles, $|C_p|_s$ is the drag coefficient of a profile, which forms part of a rectilinear series and, therefore, is under the influence of the neighbouring profiles, and $|C_R|_s$ is the lift coefficient of a profile, part of such series.

The numerical value of $|C_p|_s$ depends mainly upon $l/t$, where (t) is the blade pitch. Many experiments were carried out in air-tunnels, by Keller and others, to find values for this coefficient. The experiments show that the flow has different characteristics along the blade, according to the de-acceleration imposed on the fluid. However, conditions during such experiments differ considerably from those met in practice, and therefore, these results should be treated with reservation.

The circumferential component of the forces upon the blading cross-section is

$$T = S \sin \beta_\infty = |C_p|_s \frac{\gamma}{2g} W_\infty^2 \cdot l \cdot \Delta R \cdot \sin \beta_\infty \quad (30)$$

and also

$$T = \frac{\gamma}{g} \Delta R \cdot t \cdot C_m \cdot \Delta C_u = \frac{\gamma}{g} \Delta R \cdot t \cdot W_\infty \sin \beta_\infty \Delta C_u \quad (31)$$

from which

$$|C_p|_s \frac{l}{t} = \frac{2C}{W_\infty u} \quad .. \quad .. \quad .. (32)$$

Since

$$\Delta C_u = \frac{\Delta P}{\eta_{fl} \cdot \frac{\gamma}{g} \cdot u_m} = \frac{g \cdot \Delta P}{\eta_{fl} \cdot \gamma \cdot \omega \cdot R} \quad .. \quad (33)$$

where $\eta_{fl}$ is the aero-dynamic efficiency, and $\omega$ is the angular velocity, we may write in place of equation (32)

$$\frac{l}{t} \frac{60 \cdot g \cdot \Delta P}{\eta_{fl} \cdot \gamma \cdot \pi \cdot n} \cdot \frac{1}{R_m} \cdot \frac{1}{W_\infty} \cdot \frac{1}{|C_p|_s} \quad .. \quad (34)$$

**Aero-Dynamic Losses.**

Along a section of the impeller, having a radial height $\Delta R$, the aero-dynamic losses are:

$$|\Delta P|_r = R\,\frac{W_\infty}{C_m \cdot t \cdot \Delta R} = |C_r|_s \frac{W_\infty^2 \cdot \gamma \cdot l}{C_m \cdot 2_g \cdot t} \qquad (35)$$

and expressed percentually this amounts to

$$\left\{\frac{|\Delta P|_R}{\Delta P}\right\}_{\Delta R} = \frac{|C_r|_s}{|C_p|_s} \cdot \frac{W_\infty^2}{\frac{C_m}{u}\,u^2} \qquad (36)$$

By integration from the hub to the perifery, Keller has obtained

$$\frac{|\Delta P|_R}{\Delta P} = \frac{|C_r|_s}{|C_p|_s} \cdot \frac{1}{\psi} \cdot m, \text{ with } m = \frac{2}{3} \cdot \frac{1-\left|\frac{D_M}{D_g}\right|^3}{1-\left|\frac{D_M}{D_g}\right|^2} \qquad (37)$$

Fig. 14 shows values of m plotted against $D_M/D_G$.

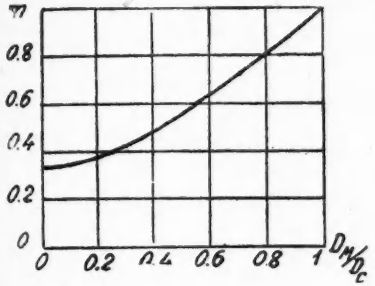


Fig. 14. Values of m plotted against the ratio $D_M/D_G$. (according to C. Keller).

The exclusive consideration of the aero-dynamic losses along the blading shows that the value of $\psi$ should be as high as possible with axial flow fans.

The losses in the diffuser may be expressed as

$$\frac{|\Delta P|_d}{\Delta P} = \frac{(1-\eta_d)\frac{c_{im}^2}{2g}}{\Psi \cdot 8/2_g \cdot u^2} = (1-\eta_d)\frac{\psi^2}{\Psi} \qquad (38)$$

The area of the output section of the diffuser is usually double of the inlet section, hence a greater efficiency than 0.8 should not be expected.

G. Keller has stated the condition for the minimum losses along the impeller and the diffuser, and derived a formula for $\psi$:

$$\frac{|C_r|_s}{|C_p|_s} \cdot \frac{m}{\psi} = \frac{4}{3}(1-\eta_d)\frac{\psi^{3/4} \cdot n_s^{4/3}}{\left[1-\left(\frac{D_M}{D_G}\right)^2\right]^{2/3}} \qquad (39)$$

The left hand side of the equation represents the losses in the impeller, the right hand side the 4/3rd of the losses in the diffuser. The minimum losses are

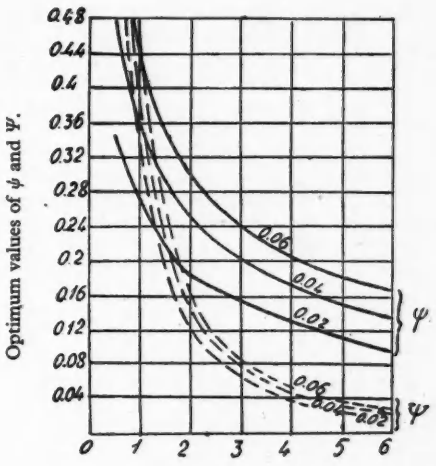


Fig. 15. Optimal values of the output coefficient $\psi$ and the pressure coefficient $\Psi$, according to C. Keller (for $|C_r|_s / |C_p|_s$ respectively = 0.06, 0.04, and 0.02.)

$$\frac{7}{4}\,\frac{m}{\psi} \cdot \frac{|C_r|_s}{|C_p|_s} \quad .. \quad .. \qquad (40)$$

The following expressions for $\psi$ and $\Psi$ can be deducted for axial flow fans

$$\psi_{opt} = \frac{n_s^2 \cdot \Psi^{3/2}}{1-\left(\frac{D_M}{D_G}\right)^2} \qquad (41)$$

$$\Psi_{opt} = \frac{\left(\frac{3}{4}\,m\,\frac{|C_r|_s}{|C_p|_s}\right)^{2/7} \cdot \left[1-\left(\frac{D_M}{D_G}\right)^2\right]^{6/7}}{(1-\eta_d)^{2/7}} \qquad (42)$$

Allowing a value for $\eta_d$=0.8, Keller has traced the diagram (15) where the optimum values of $\psi$ and $\Psi$ are plotted against the specific speed.

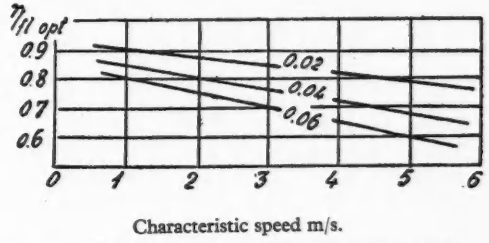


Fig. 16. Fluido-dynamic efficiency plotted against the characteristic speed, according to C. Keller (for $|C_r|_s / |C_p|_s$ respectively = 0.06, 0.04, and 0.02).

For the latter he gives

$$0{\cdot}0351 \,.\, n \cdot V^{0.5} \left[\frac{g \cdot \Delta P}{\gamma}\right]^{-0.75} = \psi^{0.5} \,.\, \psi^{-0.75} \cdot \left[1 - \left(\frac{D_M}{D_G}\right)^2\right]^{0.5} \quad (43)$$

This diagram gives useful indication for the first approximation, together with diagram 16 which shows the optimum values of the aerodynamic efficiency, and with Fig. 17 which shows the minimum advisable values for $D_M/D_G$.

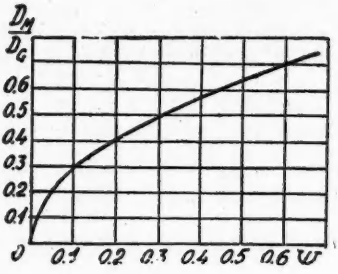


Ratio of hub diameter to impeller diameter, plotted against the pressure coefficient (C. Keller).

Fig. 17

## WIND POWER PLANTS

*Whereas utilization of water power has already reached a high degree of development, utilization of other sources of energy, e.g., of wind power, is still at the beginning of its evolution. Though the windmill has existed long before the turbine, the windwheel, suitable for the production of great quantities of energy, is a recent development. In the following three abstracts it will be shown that, in countries with no electric distribution system, considerable development has been achieved in the use of small wind motors. Furthermore, the construction of large wind power plants intended to supply wind-borne energy into large, modern networks, may be realized in the near future.*

### WIND MOTORS FOR THE TROPICS.

By H. WITTE, Berlin. (From *Elektrizitatswirtschaft*, Vol. 40, No. 1, January 5th, 1941, p. 14. Abstract from a paper read in Stuttgart, December, 1940).

THE special suitability of wind wheels is stated for countries in which there are no electrical distribution systems, e.g., in tropical regions. The conditions in these countries, so far as the wind is concerned, are said to be favourable in general for wind motor plants, e.g., a great part of East Africa is situated within the zone of the very uniform monsoon winds, which have an average velocity of 4.5 to 5 m/sec. near the ground. Of course the output of a wheel of a diameter of 20 m. is too small at this velocity for practical work. But at a velocity of 10 m/sec. 80 kW can be produced by the plant. One can expect to produce 12,500 kWh yearly with a generator of 50 kW output. For the calms standby machines (locomobiles or Diesel-engines) or a battery have to be used. A battery of 200 ampere-hours, when discharged in 10 hours, will be sufficient. It is expected that when manufactured in series, wind motor plants will be installed for £40 per kW inclusive of the charges of transport. As then the total cost will amount to ¾d or even a little less per kWh, the economy will be quite good under the favourable wind conditions of tropical regions, especially when the electric energy can be used just according to the possibility of generation, a procedure, which will be practicable for independent farms.

### THE USE OF WIND POWER IN FARMS OF THE SOVIET UNION.

By DIMITRI STEIN, Berlin. (From *Electrizitatswirtschaft*, Vol. 40, No. 4, February 5th, 1941, pp. 54/7).

RESEARCH on all questions connected with the utilization of wind power had been started in Russia in 1918. In 1931 a special Institute, The Central Institute for Wind Energy, had been entrusted with the investigation of the aerodynamic problems of the windwheel, the improvement of its regulation and the study of driving d.c. and a.c. generators by wind motors. These studies were so successful that in 1935 a great deal of the technical and scientific questions were solved so far that the construction of wind motors up to 1000 hp output could be started. Moreover, a wind motor was built with a regulation designed by Prof. Sabinin and Dr. Krasowski, which adjusted constant speed of the wheel with an accuracy of 1.5 to 2.5%. Such a motor is working successfully somewhere in an arctic country. Wind motors driving electric generators worked satisfactorily too. The wind power station 2, according to Russian sources the second

largest in the world, has been working since 1930 without interruption. It produced 8,500 kWh during the first 20 days of December, 1939.

Since 1935 the People's Commissariat for Rural Economy has been entrusted with the development of wind motors up to 100 h.p. in regard to the great importance of wind power for agriculture. Russian agriculture would have consumed $21.5 \times 10^9$ kWh in 1938 if it had been completely electrified. The real consumption was only $382 \times 10^6$ kWh or 1.78%. These figures show the extent of development which may be expected. It is intended to develop wind motors for farming on a great scale.

Though the wind is not a constant source of energy it is a very suitable one for water supply and grinding. $418 \times 10^6$ kWh could have been used in Russia for watering the cattle in 1938. The estimate for 1942 amounted to $630 \times 10^6$ kWh. The production of all windmills was expected to be $195 \times 10^6$ kWh in 1938 and $432 \times 10^6$ kWh in 1942, that is 31 or 68% of the real need.

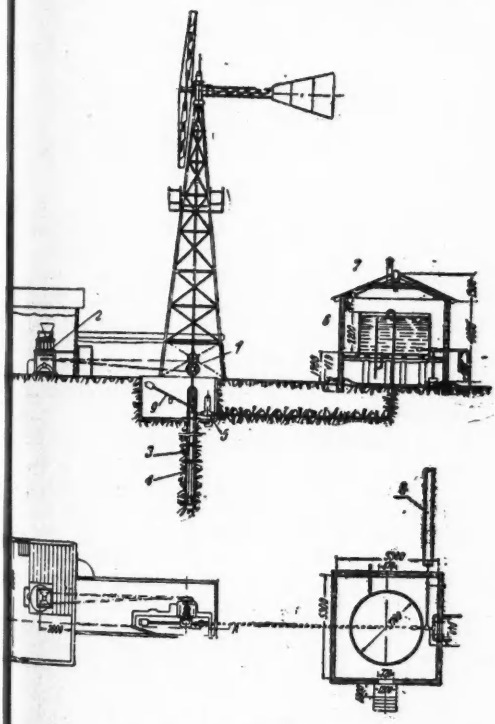

Fig. 1. Wind power plant TW—8 for water pumping and grinding.

(1) Gear
(2) Grinding plant
(3) Pump
(4) Protective tube
(5) Air vessel
(6) Tank for 20 m³ water
(7) Preheater
(8) Water-trough for cattle

Among the various types of wind motors which have been developed during recent years, the motor TW-8 is regarded as the type which has the best prospect. This motor is manufactured in great quantities and it was intended to have installed in Russian farms 9,000 such motors by the end of 1942.

**Characteristic Figures for Wind Motor TW-8.**

Nominal output of the wheel at a wind velocity of 8 m. per sec. and 25 rev. per min. .. .. .. .. 6.5 h.p.
Weight of the motor exclusive tower .. 1950 kg

Price loco factory, when manufactured in great quantities, 4,000 Rubel. Yearly production of one motor at an average wind velocity:

| | | |
|---|---|---|
| Of 4 m.p. sec. | .. .. | 9450 kWh |
| „ 5 „ „ „ | .. .. | 15000 „ |
| „ 6 „ „ „ | .. .. | 21000 „ |

As shown in Fig. 1 this wind motor can be used for the supply of water or for grinding. Water is pumped to a height of 30 m., the daily consumption is 30 to 15 m³ according to the season. This quantity is sufficient for a live stock of 1500 cattle, 300 sheep and 200 pigs. For windless days water is stored in a tank with a content of 20 m³. For longer calms the pump can be driven by horses, the cost of a TW-8 plant as shown in Fig. 1 amounts to 19,700 Rubel.

Table 1 contains some figures on the output of a TW-8 wind motor and the cost of water pumping and grinding, based on the cost of the plant mentioned before. Even at an average wind velocity as low as 4 m. p. sec. the plant works more economically than a petrol engine.

During the first years of more extensive use of wind motors, which started in 1936, some difficulties were caused by failures in the manufacturing and by the lack of trained staff. The inadequateness of manufacturing was corrected very soon. Moreover, instructions were worked out to ensure the right planning of the plants. The need of trained attendance is to be filled in the future by schooling of a great number of young people.

Wind motor plants are working successfully in a great number of collective farms in the Soviet Union. In 1936 3 plants of the type BD 8 were

installed on a government farm in the Ukraine. They provide a stock of 3,000 cattle with water. A yearly saving of 32,400 Rubel is achieved by these 3 wind motor plants.

TABLE I.

Yearly production of a TW-8 plant.

| | | Average wind velocity m. p. sec. | | | |
|---|---|---|---|---|---|
| | | 3 | 4 | 5 | 6 |
| Yearly production | HPh | 5000 | 9200 | 13300 | 16900 |
| Yearly supplement by horse drive | ,, | 500 | 300 | 200 | 150 |
| | | 5500 | 9500 | 13500 | 17050 |
| Energy necessary for the supply of 8100 $m^3$ water yearly | ,, | 1390 | 1400 | 1390 | 1390 |
| Energy disposable for grinding | | 4110 | 8100 | 12110 | 15600 |
| Quantity of grain, which can be grinded with this energy (20 kg per HPh) | ton | 82.2 | 162.2 | 242 | 312 |
| Cost of 1 HPh useful work | Rubel | 1.025 | 0.54 | 0.36 | 0.28 |
| Cost of the lift of 1 $m^3$ water to a height of 30 m | Kop. | 17.7 | 9.3 | 6.2 | 4.8 |
| Cost of grinding of 1 ton grain | Rubel | 51 | 27 | 18 | 14 |

## WIND DRIVEN GENERATOR TO GRANDPA'S KNOB.

(From *Power*, Vol. 85, No. 6, June, 1941, pp. 56/9 and 90; and *Electrical World*, Vol. 115, No. 14, April 5th, 1941, pp. 77).

A LARGE wind driven generating unit, the largest ever built and the first to deliver a.c. for commercial use is now being installed at Grandpa's Knob, in the Green Mountains about 10 miles west of Rutland, Vt., with the expectation of going into operation shortly. The installation is admittedly experimental, but it is made on a scale which should test the feasibility of such units for utilizing winds in favourable locations.

A structural steel tower (Fig. 1) supports the generator equipment at a height of about 110 ft. Nearby a 180 ft. anemometer tower has been erected (at left on Fig. 5) for temporary measurements and records of wind velocities in the experimental period. Several of the 19 instruments mounted on this tower are gas heated anemometers for measuring wind velocities even during severe ice storms.

A model of the machine plant is shown in Fig. 2. A heavy plate steel girder structure, called the pintle girder, forms the foundation of the generator plant. It can be seen in the state of being hoisted to the top of the tower in Figs. 4 and 5. It inclines downward toward the wind at an angle of 12.5 deg. The pintle girder is supported at A (Fig. 1) on the top end of the pintle shaft. This shaft has a double roller guide bearing put below the girder at B and a combined roller and trust bearing at C, which leaves the whole plant free to yaw (swing) with the wind.

The blades constructed of shot-welded stainless steel are 11 ft. wide and 65 ft. long and weigh 15,300 lb. each. Weight of the blades may double during an ice storm. The ice may heavily unbalance the two blades. Heavy centrifugal forces must also be taken into account in addition to various aerodynamic forces produced by winds up to 140 m.p.h. Normal speed of the blades, which span 175 ft., is 28.7 r.p.m., corresponding to a circumferential velocity of 263 ft. p. sec. At normal speed centrifugal forces hold the blades at nearly right angles to the main shaft. If a sudden gust of wind hits them they can cone down-wind to a maximum of 20 deg. to relieve the shock and assist the governor in regulating the speed. Speed is regulated by the governor changing the pitch angle of the blades into the wind by a mechanism similar to that employed in Kaplan turbines. Change in blade pitch angle for normal operation will be about 30 deg., but a range of 99 deg. has been provided for research purposes. The structural steel A-frames supporting the blades are shown in Fig. 3.

Two double roller bearings, one suitable to take the axial trust, support the turbine shaft, which is about 24" in diameter. The turbine

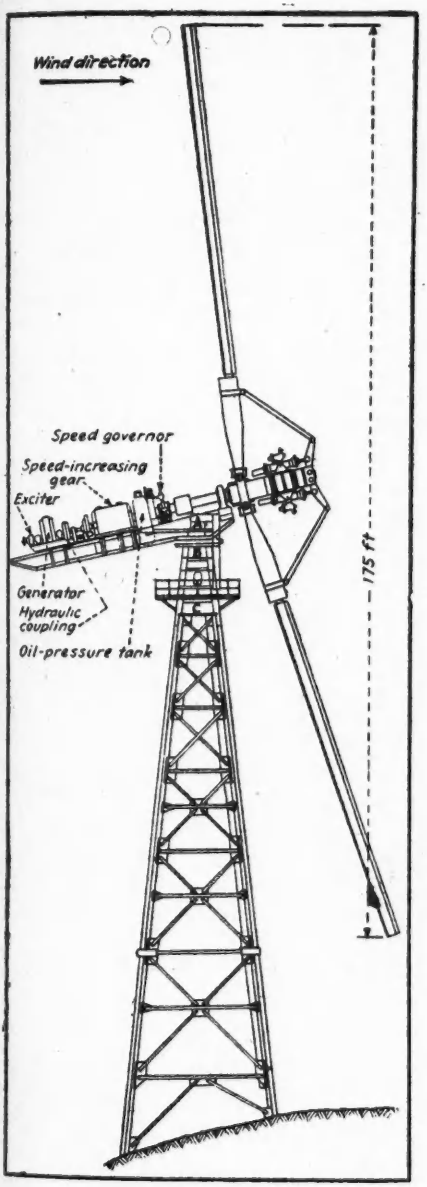


Fig. 1. The entire plant is built on a heavy structural-steel pintle girder on top of a 110 ft. tower anchored by a heavy steel and concrete foundation.

shaft couples to a gear that increases the speed to 600 r.p.m. Connecting the gear to generator is made by an American Blower hydraulic coupling. The governor, a standard Woodward speed governor, is gear driven from the turbine shaft. On the output-gear shaft, between the gear case and the hydraulic coupling, a friction clutch gears into a motor driven turning device equipped with a brake. When the unit is shut down, the clutch can be closed and the brake on the turning device applied to prevent the turbine from turning. This turning device will also serve to put the machine rotor to any desired position, when the unit is shut down.

At all times the unit is held with the turbine down-wind by a hydraulic mechanism controlled by a yaw meter (wind direction vane) mounted on the housing, that will enclose the generator equipment on the pintle girder.

The generator, built by the General Electric Company, is rated 1000 kW at 80% p.f., 2,300 V, 60 cycles, three-phase. Leads are taken down through the centre of the pintle shaft and are connected to slip rings. Energy will be raised to 44 kV for transmission into the Central Vermount Public Service Corp. system over a 4 mile tie line.

It is expected that favourable wind will be available to operate the unit about 4,000 hours per year, about 2,700 hours of which will be at full load. This is on the assumption that the unit will go into service at a small percentage of rated capacity, when the wind reaches a velocity of 18 m.p.h., and will be taken out of service at wind velocities above 60 m.p.h.

Control of the station will be entirely automatic, using very much the same equipment as in automatic hydro-electric plants. Starting and stopping of the unit will be done automatically according to the velocity of the wind.

The unit has unusually high unit inertia and should, therefore, be exceptionally stable in operation. The only way this characteristic can be obtained in a wind power unit, is by building in a heavy fly-wheel or by building units of comparatively large sizes. All studies made of the problem indicated that the solution of speed regulation of wind turbines is inherently associated with large size units. For this reason a 1000 kW machine is being installed instead of a small experimental unit. But even with this large unit it is difficult to predict what will be the effect of sudden changes in wind direction and velocity combined with abrupt load changes. The hydraulic coupling has therefore been in-

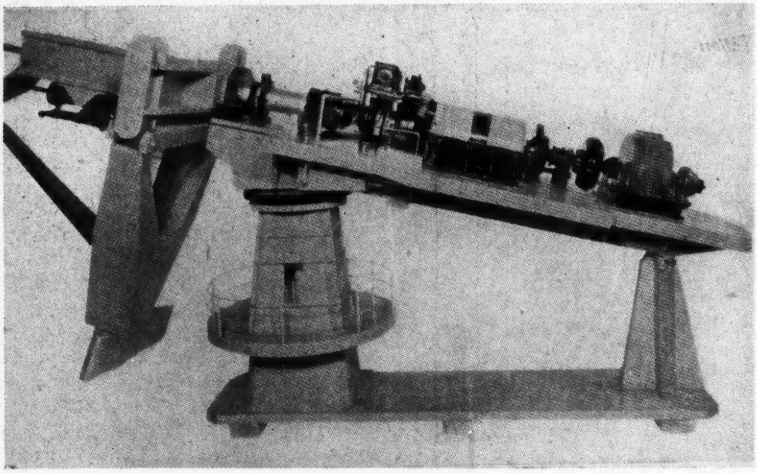

Fig. 2. Model of the generating part with a part of one blade.

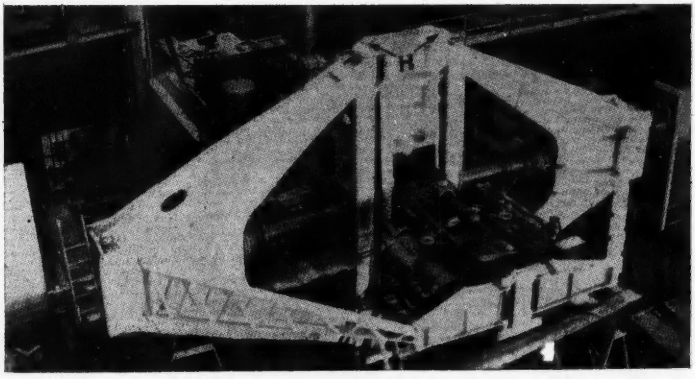

Fig. 3. Structural-steel A-frames supporting the blades.

stalled to act as a slip connection and to prevent sudden overloads. If this coupling is found unnecessary, it may be omitted in future designs. The designers of the plant were pioneering in a field where fundamental knowledge and practical experience are lacking. Therefore, wherever they were in doubt, they provided against every possible emergency they could think of.

Palmer Cosslett Putnam is the inventor of the plant. He worked out the general design, having begun the study on wind power in 1935. In 1939, E. Smith, of S. Morgan Smith & Co., assumed the financial responsibility for the project. Moreover, this firm is supplying the designs of the mechanical equipment with the aid of various specialists and the Wellman Engineering Co. T. S. Knight, Vice President of the General Electric Company, agreed to collaborate with Putnam in working out the detailed project.

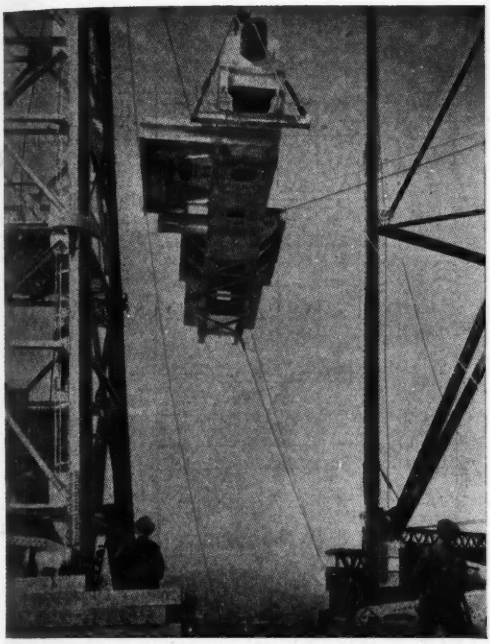

Fig. 4. The pintle girder, weighing nearly 50 ton, is hoisted to the top of the 110 ft. structural-steel tower.

Fig. 5. Here the girder is being lowered into the place on to the top end of the pintle shaft supported in the tower by two holding roller bearings. The heavy timber strut jutting out from the left hand side of the tower will support temporarily the free end of the pintle girder during erection of the plant. In the left hand background can be seen the 180 ft. high anemometer tower equipped with 19 instruments.

# HYDROGEN CONTENT, SOLUBILITY, PERMEABILITY AND ITS EFFECT UPON FLAKE FORMATION IN STEEL.

By HUBERT BENNEK and GUNTER KLOTZBACH. (From *Stahl und Eisen*, Vol. 61, Nos. 25-26, June, 1941, p. 597 and continued).

FLAKES are separations of material caused by the pressure development of hydrogen blowholes or occlusions in steel, when the hydrogen content surpasses the limit of solubility at low temperatures and cannot escape from the metal by diffusion. A quantitative analysis of the relation between hydrogen content and flake formation could not be successfully carried out as long as opinions on the various methods of determination of hydrogen content differed.

A consideration of these methods led to the method consisting of the extraction of hydrogen in a quartz tube at elevated temperatures after melting the steel specimen with tin at about 1100 to 1150°C., suitable apparatus being developed. The limits of accuracy of this method were examined and it was found that the results could only be used as comparative values, and, even then, only if the specimens were obtained by identical production processes, as losses of hydrogen may occur during the manufacture of the specimen.

*Permeability of Various Steels to Hydrogen.*

The analysis of the steels investigated and their capacity of hydrogen absorption at 950°C is given in Table I. Besides certain carbon steels several alloy steels inclined to flake formation were examined.

Investigations with regard to hydrogen content revealed that the rate of hydrogen emission varies with different steels. This can be best illustrated by diagrams similar to Fig. 1. The inclination of the lines depends upon the change of rate of

TABLE I.

| Steel | C % | Si % | Mn % | Cr % | Mo % | Ni % | Other elements % | Absorption of hydrogen at 950°C in cm³/100 gr. |
|---|---|---|---|---|---|---|---|---|
| 1 | 0,03 | 0,01 | 0,12 | — | — | — | — | — |
| 2 | 0,13 | 0,14 | 0,35 | — | — | — | — | 5,64 |
| 3 | 0,47 | 0,26 | 0,71 | — | — | — | — | — |
| 4 | 0,99 | 0,31 | 0,45 | — | — | — | — | 4,97 |
| 5 | 0,21 | 0,24 | 0,47 | 0,72 | — | 3,62 | — | — |
| 6 | 0,13 | 0,30 | 0,40 | 1,52 | — | 4,11 | 1,03 W | 5,56 |
| 7 | 1,06 | 0,42 | 0,30 | 1,53 | — | — | — | 5,61 |
| 8 | 0,25 | 0,24 | 0,90 | 2,68 | 0,24 | — | — | 5,70 |
| 9 | 0,10 | 0,67 | 0,40 | 1,80 | — | 8,9 | — | 7,60 |
| 10 | 0,24 | 0,28 | 0,90 | 2,72 | 0,26 | — | 0,52 Al | 5,84 |

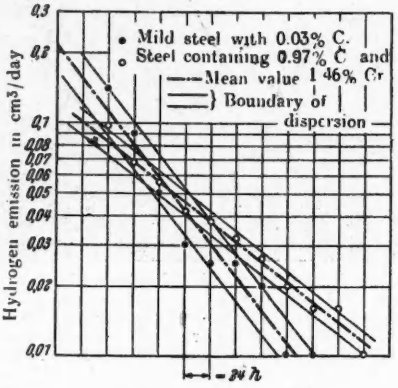
Hydrogen emission in cm³/day
• Mild steel with 0.03% C.
o Steel containing 0.97% C and
Mean value 1.46% Cr
Boundary of dispersion
24 h

Fig. 1

emission of the gas, and is in consequence a measure of the permeability of the steel. In agreement with other publications the authors showed that the rate of hydrogen emission depends on the structure of the specimen in so far as hydrogen escapes at a slower rate with increasing martensitic structure; the influence of the alloying metals is only of indirect importance by inducing the formation of martensitic structure. Austenitic steel forms an exception, as with this metal no gas emission takes place at normal temperatures. Fig. 2 is a typical illustration of the variation of permeability to hydrogen with temperature. The transformation points are clearly marked and the inclination of the lines in the $\gamma$ and $\alpha$ region differ considerably, as can be seen more clearly from the extrapolated curves in Fig. 3. The permeability to hydrogen in the $\alpha$ region is at 700°, 4.16 times, at 500°, 14.5 times, at 300°, 107 times and at 100°, 7650 times that of the $\gamma$ region at corresponding temperatures. On comparing such curves obtained for various steels, it was found that the difference of inclination of the lines representing the $\alpha$ and $\gamma$ region was the same.

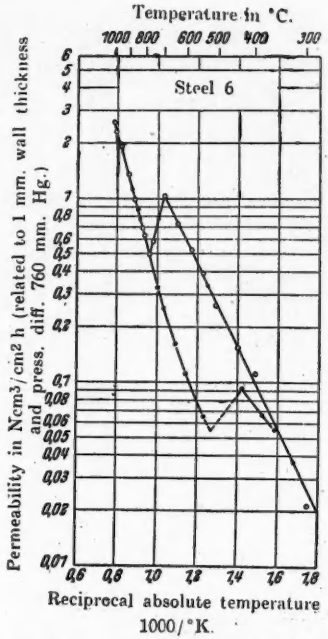
Temperature in °C.
1000 800 600 500 400 300
Steel 6
Permeability in Ncm³/cm² h (related to 1 mm. wall thickness and press. diff. 760 mm. Hg.)
Reciprocal absolute temperature 1000/°K.

Fig. 2. Steel 6, containing 1.52% Cr, 4.11% Ni, and 1.03% W.
° = heating
• = cooling-down

When using these lines for the determination of the tendency to flake formation it must be remembered, however, that the curves so obtained correspond to retarded cooling in the furnace, as it was necessary to keep the temperature constant for about two hours at each stage for the sake of measurements. Under conditions met in practice the $\gamma$ region is sustained down to much lower temperatures, and the permeability will fall more rapidly with decreasing temperatures corresponding to the $\gamma$ line.

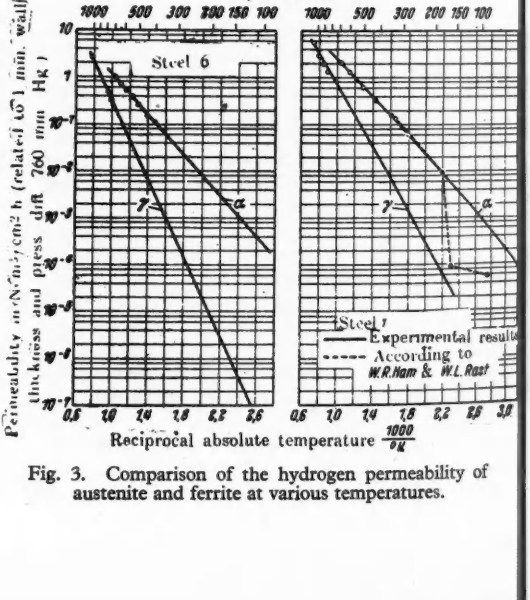


Fig. 3. Comparison of the hydrogen permeability of austenite and ferrite at various temperatures.

*Solubility of Hydrogen in Steels of Various Composition.*

The solubility of hydrogen in steel at low temperatures cannot be readily determined on account of the small value of the permeability under such conditions. It seems clear, however, from all that is known in this respect, that it is sufficient, for our purpose, to determine the hydrogen solubility in steel at temperatures above the $\gamma/\alpha$ transformation. As Table I shows, the solubility of hydrogen in the investigated steels at 950° C is practically the same. The small deviation of steels No. 4 and 9 is without significance and may be explained by the higher hydrogen solubility in nickel than steel.

Rapid cooling of specimens of various steels and alloys seems to indicate that the solubility in alloy steels is considerably higher than that in carbon steels; the difference amounts to nearly 50%. This phenomenon is the result of the difference of permeability of steel for carbon steels and steel alloys. The $\gamma/\alpha$ transformation takes place for the carbon steels at a temperature when there is still a comparatively high permeability, while for the alloy steels, the point of transformation is shifted to lower temperatures, i.e., to a point of lower permeability, where the hydrogen content, though rejected, cannot occlude from the alloy.

*Hydrogen Content and its Influence upon Flake Formation.*

The great difficulty in the determination of the hydrogen content necessary for flake formation is obvious from the aforegoing. Hydrogen may escape during production, and also while the molten metal for the samples is taken; the amount of hydrogen that escapes this way cannot be estimated. Therefore, another method of investigation has been developed. This consists of the determination of hydrogen content of specimens taken during casting and poured into moulds of such size that no further working is necessary. Again, in this case, a comparison could be made only between specimens of the same steel. The conclusions could not be applied to other steels without reservation and consideration of the different conditions of cooling. The steel was heated in a high frequency furnace, and in some cases hydrogen was blown into the molten metal through a quartz tube. The investigated steels corresponded to the steels Nos. 2, 4, 5, 6, and 7 of Table I. The specimens were either taken during casting, or by sawing and turning discs of 9 mms. diameter and 35 mm. length. As could be expected, all steels without artificial addition of hydrogen were free of flakes, but an interesting result was that the hydrogen content did not increase with increasing duration of blowing hydrogen into the molten metal. The fluctuation of hydrogen content may be explained by the different melting temperatures, humidity, lining of the furnace, or by the fact that part of the hydrogen added was being used for reduction of oxides.

In case of the alloy steels, the castings showed generally an increasing inclination to flake formation with increasing hydrogen content, provided the quantity of hydrogen emitted up to 400° C was considered only. This characteristic could not be detected between 400° and 1150° C. Flake cracks could not be detected in the carbon steels. A similar investigation of the forged ingot specimens did not reveal any such relationship between the various factors, because a considerable change of the hydrogen content took place as a consequence of forging.

A careful consideration of the figures of the hydrogen contents showed a different proportion of the hydrogen quantity emitted (a) below 400° and (b) between 400° and 1150° C, to the total quantity emitted for the various steels. With the steels 5 and 6, part (a) increases with increasing total hydrogen content, but with steel 7 the proportion (b) increases. In case of the carbon steels, both parts (a and b) are equally affected.

An explanation to this behaviour as far as part (a) is concerned may be given by the different conditions for the hydrogen emission during cooling of the forged specimens. The speculations regarding part (b) have a very unreliable foundation and will be, therefore, omitted.

*Conclusions on the Conditions Resulting in Flake Formation.*

It is now clear that for flake formation a certain amount of hydrogen is indispensable. If cooling is slow, the hydrogen can diffuse from the material without difficulty. As cooling proceeds, however, the permeability to hydrogen decreases, and this decrease is much more rapid in the $\gamma$ region than in the $\alpha$ region. As soon as the $\gamma/\alpha$ transformation takes place, a large quantity of hydrogen is suddenly released. If the temperature is still high enough the hydrogen can escape from the steel, especially as an increase of permeability is connected with the transformation. If, however, influenced by alloying elements, or by the cooling rate, the transformation takes place at lower temperatures, the hydrogen is released only at a time

when the permeability of the steel has greatly decreased. If the resulting gas pressure surpasses the strength of the material, flake formation takes place. Stresses resulting from the formation of martensite, or from cooling, determine first of all the location of the flakes in the material, but may, of course, contribute to the stresses caused by the gas pressure and thereby favour flake formation.

It is generally agreed that flake cracks can be avoided by arranging for a slow rate of cooling; a better method is a preliminary deformation with intermediate annealing at a temperature just below the transformation temperature and subsequent forging. In this case the annealing times are comparatively short. Longer arrest times are necessary at lower temperatures, and at about 700° the formation of flakes cannot be completely avoided even with long arrest times. This phenomenon is in confirmity with the results of the above mentioned experiments on permeability and solubility. In consequence a method is recommended where the $\gamma/\alpha$ transformation takes place at temperatures as high as possible, i.e., annealing with pearlitising result. The hydrogen released at the transition from the $\gamma$ to the $\alpha$ region can escape from the steel owing to good permeability. In order to improve the permeability, the steel can be heated to just below the transformation temperature (after transformation); however, the mixed crystals have such a high solubility that the hydrogen remaining in equilibrium will still be sufficient to cause flake formation during subsequent cooling.

## STRESS CRACKING CAUSED BY HYDROGEN & INTERNAL STRESSING

By EDUART HOUDREMONT and HANS SCHRADER. (From *Stahl und Eisen*, Vol. 61, No. 27, July, 1941, pp. 649-653).

THE formation of cracking in steel is the result of

(1) Stresses originating from (a) temperature differences during cooling; (b) deformation; (c) transformation and

(2) Casting technique (a) impurities; (b) segrations; (c) gases.

Individually, no single factor is directly responsible for the formation of flaws. It has been enphasised, frequently, that the presence of hydrogen is the primary factor in the development of this imperfection, consequently all the other factors have only an aggravating effect. It is the purpose of this article to correlate the experiments on the influence of these secondary factors.

A series of publications have confirmed the influence of hydrogen upon flake formation. They deal partly with investigations on steel, where hydrogen has been absorbed by the molten metal, and partly with steel that has been annealed in a hydrogen atmosphere or has been exposed to hydrogen during the normal production processes, e.g., cutting by oxy-hydrogen torch, quenching of ball bearings after cementation in a salt bath at comparatively high temperature.

The influence of temperature and duration of annealing in a hydrogen atmosphere can be studied from Fig. 1 and needs no further explanation.

### Influence of Various Rates of Cooling.

The experiments have confirmed a series of facts, mostly well-known, and used in practice for avoiding, or at least diminishing, the formation of stress cracking, e.g., slow cooling of forged and rolled ingots in a furnace.

The number of stress cracks diminishes with decreasing cooling rate, especially for Cr-Ni steel, where the cooling in ashes is not sufficient to hinder the development of flake formation, while similarly treated manganese steel revealed many cracks with water quenching, sporadic cracking with oil quenching, and no cracking with less drastic cooling. Carbon steels are still less sensitive. There are two alternative explanations to this behaviour; if the rate of cooling is slow, there

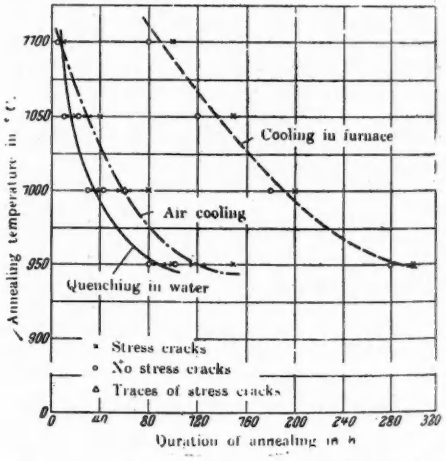


Fig. 1. Relation between temperature and duration of annealing for development of stress cracks by annealing in a hydrogen atmosphere, with three different rates of coolings, for specimens of 60 × 60 mm. square section containing 0.34% C, 0.28% Si., 0.53% Un, 0.38% Cr, and 4.50% Ni.

is ample time for the hydrogen to diffuse out of the steel. Alternatively, at high rate of cooling, the stresses caused in the material might assist in the development of cracks. Although experiments have shown that the first mentioned explanation may not be accepted at its face value, nevertheless, in the complete absence of hydrogen no cracks are formed, no matter how drastic the cooling rate. Furthermore, the temperature was determined at which stress cracking takes place in a Cr-Ni steel, saturated with hydrogen by annealing in a hydrogen atmosphere and cooling in a furnace to room temperature. The number of cracks decreases with decreasing quenching temperature and steel quenched from 600° C is free from cracking.

**Effect of Stressing on the Formation of Stress Cracks.**

Detailed experiments carried out on steels of various composition have shown that stresses alone cannot produce cracks in a steel free of hydrogen; but in the presence of hydrogen, stressing can greatly influence the direction of stress cracking the nature of which differs frequently, according to the shape of the article. Overstressing may cause cracking even when the hydrogen content is less than that which induces cracking at the particular rate of cooling. It is obvious that hydrogen content and stressing cooperate to cause stress cracking, but it is still questionable whether a critical cooling rate is an essential factor.

**Martensite Transformation and Flake Formation.**

From what is known of the influence of stressing, it is obvious that a partial transformation to martensite and the accompanying stressing can produce stress cracking if the necessary hydrogen is present. The question arising is whether transformation is an essential factor in the formation of stress cracking? On hand of experimental results it can be concluded that transformation stresses and formation of martensite are not indispensable conditions for the development of stress cracks, as these can be obtained in steel of 4% Si content, which is considered to be free from transformation points. Similar results were obtained with steels charged with hydrogen below the transformation temperature.

## EXAMINATION OF A CRANKSHAFT AFTER ONE MILLIARD REVOLUTIONS

By Dr. Ing. Karl Daeves and Dr. Gotthold Becker. (From *Die Wärme*, Vol. 64, No. 20, 17th May, 1941, pp. 205-206).

The examination of machine parts after many years' service throws light upon the discrepancies between the subsequently found properties of metal and those specified for the fabrication. If these discrepancies are not within the allowable limits, the specifications should be modified accordingly.

The crankshaft investigated was used in a big electric plant, and was the mechanical coupling between the gas engine and the dynamo. It was first put into commission in 1914, where it remained until 1939, when owing to a minor breakdown it was dismantled and repaired. The dimensions of the crankshaft can be seen in Fig. 1. During its 25 years' service it is estimated that it has performed over 1 milliard revolutions.

The mean shear in the crankshaft during operation was about 86 kg/cm², with peak values of about 343 kg/cm². Although these figures appear to be low considering the size of the shaft, it should

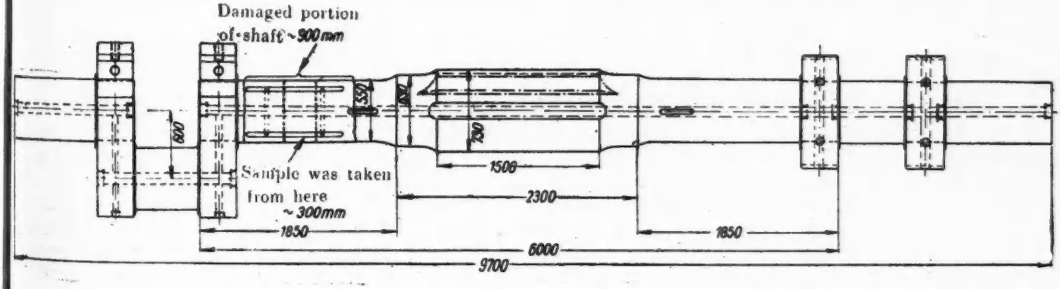


Fig. 1

TABLE I.

| Sample | Sector | Limit of elasticity kg/mm² | Tenacity kg/mm² | Elong. 1=5d | Impact strength mgk/cm² | % Reduction of Area |
|---|---|---|---|---|---|---|
| Edge, longit. | 1 | 27.4 | 46 | 30.8 | 9.5 | 65 |
| | 3 | 23.4 | 43.2 | 32.5 | 8.8 | 65 |
| Middle, longit. | 1 | 22.8 | 41.8 | 31.7 | 4.0 | 61 |
| | 3 | 20.9 | 41.0 | 32.5 | 3.0 | 60 |
| Edge, tangential | 1 | 25.0 | 44.4 | 26.7 | 4.0 | 41 |
| | 3 | 22.1 | 43.9 | 26.7 | 3.4 | 45 |
| Edge, radial | 1 | 21.2 | 41.4 | 25.8 | 3.5 | 36 |
| | 3 | 20.6 | 40.8 | 23.3 | 3.3 | 37 |
| Middle, radial | 1 | | | | 1.3 | |
| | 3 | | | | 1.5 | |

be remembered that in gas engines higher peak loads may occur due to pre-ignition, and, in addition, the great weight of the dynamo armature was responsible for considerable bending moments.

From the centre of the damaged part, a piece, 300 mm. long, was sawn out, divided into four quadrants and examined. The chemical analysis showed the following composition:

| | C% | Si% | Mn% | P% | S% |
|---|---|---|---|---|---|
| Middle portion .. | 0.18 | 0.07 | 0.93 | 0.057 | 0.046 |
| Peripheral portion | 0.19 | 0.06 | 0.95 | 0.067 | 0.045 |

Two quadrants were used for preparing samples for tensile and impact strength examination. The samples were taken from the shaft part along radial, longitudinal and tangential directions, from the middle and the periphery of the quadrants respectively. The results are tabulated in Table I.

The impact strength, especially at the middle portion, is very low, but has apparently little or no effect upon the strength of the crankshaft.

The Bauman impression test is shown in Fig. 2 and presents a uniform colourisation except for the case hardened peripheral ring. Microscopic examinations revealed a uniform ferritic-pearlitic structure.

**Conclusion.**

The present results, corresponding to other similar investigations, reveal a distinct discrepancy of analysis limits and impact strength from the figures specified by the manufacturer. Since the failure of the shaft is by no means a result of these weaknesses, the impact strength figures should be treated with reservation by the engineers, as they do not seem to constitute a deciding factor for their suitability of application.

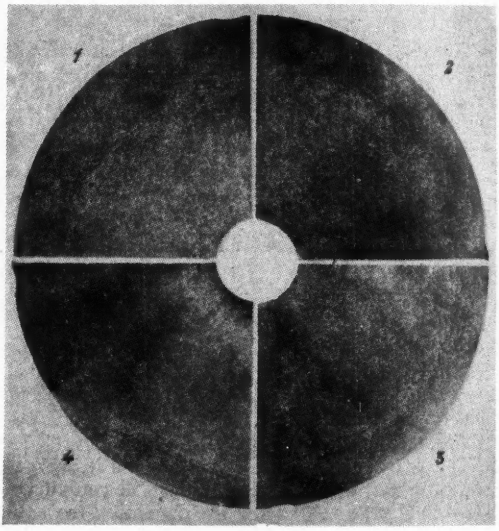


Fig. 1

## DESIGN OF MECHANISMS FOR ENDURANCE STRENGTH

By H. MADING. (From *Werkstatt und Betrieb*, Vol. 74, No. 8, August, 1941, pp. 201-204).

A MECHANISM subject to a fluctuating load, superimposed on a static load is liable to fail in service by fatigue. The fluctuating force, of course, might also be induced by an unbalanced rotating mass or by resonance. After static tests on the fractured part fatigue failure can be recognised at once as such, since the safety factor corresponding to the static loading will be excessively high. On the other hand, it would be a gross mistake to attribute every failure to fatigue, since, in many instances, other factors are dominant, as for instance, a worn out bearing.

In effect, the problem is to determine the safety factor of the application. The strength of the

mechanism is affected by two considerations.

1. The number of load reversals up to a definite number after which no further reduction in fatigue resistance takes place.

2. The shape and form of the machine part.

Fig. 1 shows a typical Wöhler curve. In this

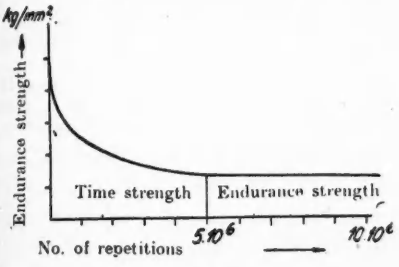


Fig. 1

particular case the critical number of repetitions is $5 \times 10^6$. It is understood, of course, that this figure will vary with different materials. The endurance strength of a material will be that figure which corresponds to the limiting number of repetitions on the Wöhler curve. Naturally, if the maximum number of reversals is known for a particular application, then the limiting stress will be the one corresponding to the number of reversals, and the property of " time strength " is introduced.

Fig. 2 shows the endurance-strength curve, originated by Smith, which has become very popular in Germany during the last few years. There is, of course, an upper limit $\sigma_o$, and a lower limit to $\sigma_u$ to the stress. The mean stress intensity become $\frac{\sigma_o + \sigma_u}{2} = \sigma_m$, measured along the abscissae, while values of stress are measured as ordinates. The mean stress line appears as the $\sigma_m$ line at an angle of 45° to the axes; $\sigma_s$ represents the yield point and is the extreme limit of the graph. The forces acting at points I., II., and III., are purely static, " repeated," and " reversed " respectively. The force between points I. and II. is a combination of a fluctuating and a static force, and that between points II. and III., is a combination of reversed and static force.

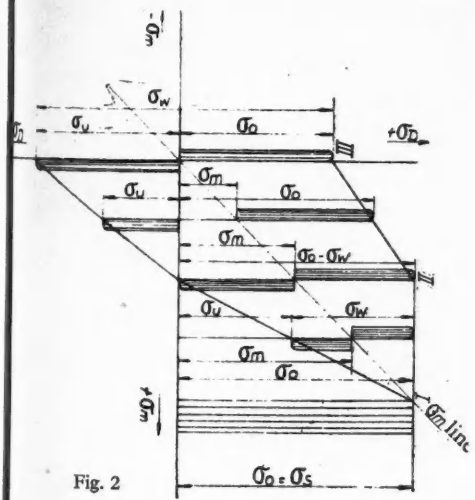


Fig. 2

When a mechanism is subject to a dynamic load it is essential to consider its fatigue strength when designing it. To do so it is not sufficient to refer to the Wöhler curve of the material used, but as suggested by Hänchen, two modifying factors must be considered allowing for the shape and finish of the article. Thus:

Maximum allowable stressing

$$\sigma_{oG} = b_1 \cdot b_2 \cdot \sigma_d$$

Tabulated values for $b_1$ and $b_2$ can be found in handbooks, compiled by various authors.*

Proceeding with the original problem, the determination of the safety factor of the design, the actual stressing occurring in the machine part need to be calculated. In this relation consideration must be given to the shape of the machine part as notch sensitivity, in particular, causes high peak stress concentration in the material; as an example,

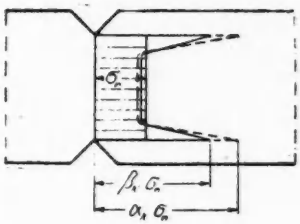


Fig. 3

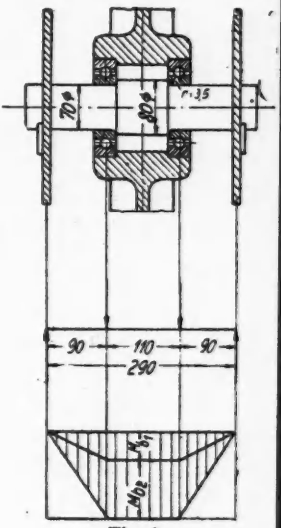


Fig. 4

Fig. 3 shows the stressing in a flat steel bar with a notch on each side. The peak stress owing to a notch can be allowed for by introducing a coefficient $\beta_k$, so that

$$\sigma_{max} = \beta_k \, \sigma_n$$

where $\sigma_n$ is the nominal stress intensity in the material.

The value of $\beta_k$, will in turn, depend upon the material used and upon the shape of the machine part. In this way, $\beta_k$ is actually the product of two separate coefficients, $\sigma_k$, the "form coefficient," and $\eta_k$ the coefficient characteristic of the material. Therefore, we get

$$\beta_k = 1 + \eta_k (\alpha_k - 1)$$

and hence, $\sigma_{max} = [1 + \eta_k (\alpha_k - 1)] \, \sigma_n$

Consequently the safety factor becomes:

$$S = \frac{\sigma_{OG}}{\sigma_{max}} = \frac{\sigma_D \cdot b_1 \cdot b_2}{[1 + \eta_k (\alpha_k - 1)] \, \sigma_n}$$

In practice, the values of $\sigma_k$ and $\eta_k$ are determined by comprehensive experiments, but once these are known, the safety factor of the design, taking account of the fatigue strength, can be readily determined.

This method of estimating the safety factor is illustrated by the following example.

**Example.** Safety factor of a shaft of St 50.11, for a carriage carried by a loosely mounted pulley. The pulley runs in two ball bearings, Fig. 4.

Useful loading=4000 kg. Weight of carriage =2000 kg. Bending moment due to carriage= $Mb_1$=1000.9=9000 cmkg. Bending moment due to useful load=$Mb_2$=2000.9=18,000 cmkg. Hence $Mb_{max} = Mb_1 + Mb_2$ = 27,000 cmkg.

Lower limit of stressing

$$\sigma_u = \frac{9000}{33.7} = 265 \text{ kg/cm}^2$$

Range of stressing

$$\sigma_w = \frac{18.000}{33.7} = 535 \text{ kg/cm}^2$$

Upper limit of stressing

$$= \sigma_u + \sigma_w = 800 \text{ kg/cm}^2$$

At the stepping from d to D on the shaft, there is a stress peak. If $\rho$ = 3.5 mm, the coefficient $\alpha_k$ = 2.0 (from tables). The coefficient of notch sensitivity of the material $\eta_k$ = 0.8, hence.

$$\beta_k = 1 + 0.8 \, (2\text{-}1) = 1.8$$

and therefore, the peak of the stress becomes 800 × 1.8 = 1440 kg/cm². The bending stress durability of this material is 3700 kg/cm² (from tables). The two coefficients, $b_1$ and $b_2$, for the particular size and finish of the article are 0.65 and 0.9 respectively. Therefore, the maximum allowable stress intensity in the material is given by

$$\sigma_{og} = 0.65 \times 0.9 \times 3700 = 2160 \text{ kg/cm}^2.$$

And finally the safety factor of the design becomes:

$$S = \frac{2160}{1440} = 1 \cdot 5$$

*Values for $b_1$ are given for bending forces by Lehr, and for twisting by Bautz (S. ten Bosch, Maschineteile, Berlin, 1940, Julius Springer). For $b_2$, values are tabulated in "The handbook for Machine design," by Dubbels, 7th edition (Julius Springer).

## MILLING OF LIGHT ALLOYS

By F. H. HURTH. (From *Werkstatt und Betrieb*, Vol. 74, No. 6, June, 1941, pp. 155-158).

EXPERIMENTS for the determination of tool reaction when milling light metals have been carried out by means of a torque measuring instrument (Fig. 1). Its operation will be understood by referring to the figure and the legend; the gauging of the instrument is illustrated in Fig. 2. A lever is placed on the milling arbor and the driving pin, the free end carries a load = $G_2$ kg. $L_1$ and l are the distances of the fulcrum from the centre of gravity and the application of load respectively. Then, if r is the radius of the milling cutter in centimetres, the tool thrust P, in kg, is given by

$$P = \frac{(Q + G_2) \cdot l + G_1 \cdot L_1}{r} \text{kg.}$$

The general formula for chipping is

$$P = K_m \, . \, b \, . \, t \text{ kg,}$$

where b is the width of the milling cutter in

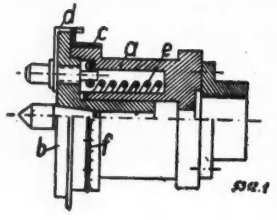


Fig. 1

a = hollow cylinder with spigot to be inserted into milling spindle.
b = rotating cover.
c = driving ring.
d = driver to C.
e = spring calibration.

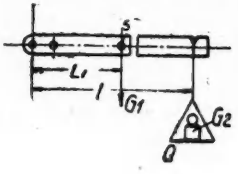


Fig. 2
Gauging of the torque measuring instrument.

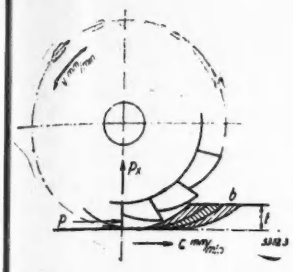

Fig. 3

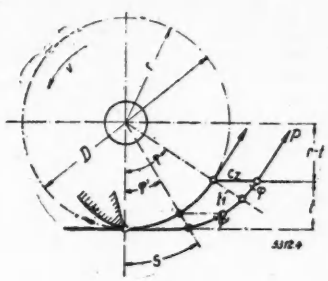

Fig. 4

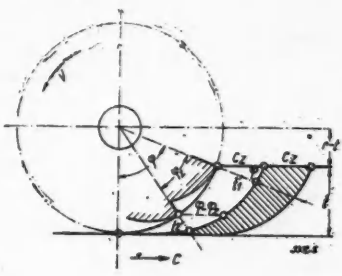

Fig. 5

mms., t is the depth of the cut in mms., and $K_m$ is the cutting resistance of 1 sq. mm. cutting plane in kg.

The work done by the cutter per minute, when the cutting speed is v, and the feed speed is c feet per sec. is:

$$P.v = K'_m \cdot b.t.c \text{ millimeter-kg.}$$

A mathematical consideration of the milling process as shown in Figs. 3 to 5 gives the same result, and shows that the maximum thickness of the chip is

$t_{max} = \frac{c_1}{z} \sin \phi$ for one tooth of the cutter (Fig. 4).

$t_{max} = \frac{c_1}{z} [\sin \phi + \sin (\phi - \phi_z)]$ if two teeth cut at the same time (Fig. 5).

$t_{max} = \frac{c_1}{z} [\sin \phi + \sin (\phi - \phi_z) + \sin (\phi - 2\phi_z)]$ if three teeth cut at the same time,

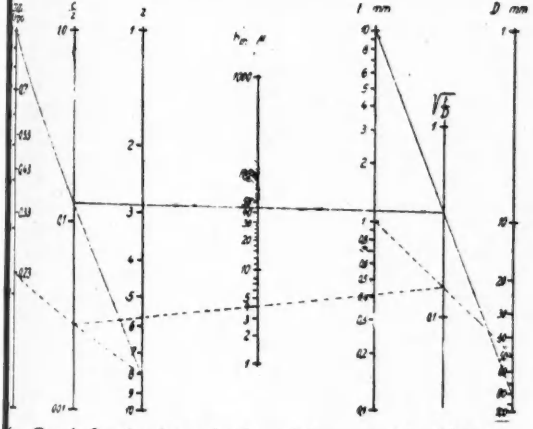

Graph for the determination of the mean chip thickness.

where $c_1$ is the feed speed per revolution in mms., and z is the number of teeth of the cutter.

The above equation for P can be written as

$$P_m = K_m . h_m$$

for the value of b=1 and $h_m = c/z\sqrt{t/D}$ millimetre.

As $h_m$ is very small it is more convenient to express it in microns $\mu$, and the calculation of the various values of $h_m$ can be greatly facilitated by using the graph (Fig. 6). Using the original equation,

$$P.v = K_m . b.t.c.$$

the values of $K_m$ can be determined for any experimental condition where the values of P, v, b, t and c are known, and can be represented by graphs plotted against the corresponding values of $h_m$. This has been done for three different light alloys, the mechanical properties of which are tabulated:

| Metal | Tenacity tons/sq. in. | % Elongation | Brinell hardness |
|---|---|---|---|
| 19 V | 16.5-22 | 12-20 | 70-95 |
| M Z B | 27-32 | 8-15 | 100-130 |
| 61 P | 11.5-16 | 10-18 | 50-60 |

Fig. 7 shows the final result when logarithmic values are plotted; in this graph lines representing St 60.11 and Cast Iron (Ge) have been entered for the sake of comparison.

The practical application of these fundamentals

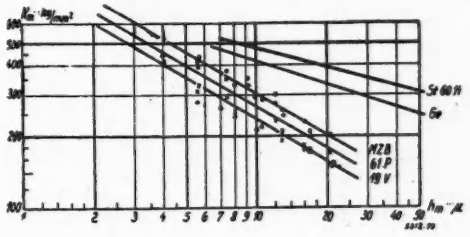

Fig. 7

is perhaps best illustrated by the following example. An article of V 19 has to be milled by a cutter of 80 mm. diameter and 8 teeth; the feed is 1 mm./rev. and the speed is 800 r.p.m. The width of the work is 30 mm., the depth of the cut 10 mm. Fig. 6 gives $h_m = 46\ \mu$ and Fig. 7, $K_m = 98.5$ kg/sq. mm. (actually this is not shown in Fig. 7 as the base line represents $K_m = 100$).

The power required for this job is then:

$$\frac{98 \cdot 5 \times 30 \times 10 \times 800 \times 1}{4500 \times 1000} = 5 \cdot 25 \text{ H.P.}$$

and if the efficiency of the driving motor is assumed to be 70%, the total power required will be 7.5 H.P.

If on the other hand the horse power of the motor is known, the cutting depth, the speed, or the feed can be determined, for economic operation.

## BEHAVIOUR OF RUBBER SPRINGS UNDER VARIABLE LOADING CONDITIONS

By Dr. Ing. F. Gobel. (From *VDI, Zeitschrift des Vereines Deutscher Ingenieure*, Vol. 85, No. 29, July, 1941, pp. 631-635).

Development of aircraft design has changed the rigid attachment of aero-engines to the fuselage to a more elastic embedding by means of rubber springs. The cylindrical rubber springs were mounted between the engine and frame in a fashion illustrated by Fig. 1. As a result the vibration transmitted to the cabin was reduced and fatigue failures owing to the rigid connection were eliminated.

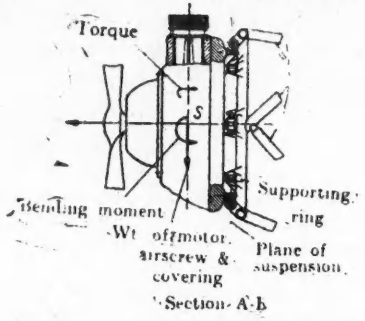


Fig. 1

The stress-deflection curves for cylindrical rubber springs are curvi-linear, and some typical curves for axial stressing are shown in Fig. 2. In practice, the stressing of such springs does not exceed values which would yield a deflection of 1.0 cm and 0.5 cm in the axial and radial directions respectively. In Fig. 3, a polar diagram for a rubber spring is shown, indicating deflections and corresponding stressing in various directions.

To establish a mathematical relationship between stiffness and spring dimensions would, of course, be of great value. It was possible to derive such a formula for spring deflections not exceeding 1 cm. Then

$$P = \frac{2\pi f\ G_i\ h}{l\ n\ d_a/d_i} \quad \ldots\ \ldots\ \ldots\ (1)$$

where P is the axial force in kg., f is the spring deflection in cm., $d_a$, $d_i$, and h, dimensions in cm., as shown in Fig. 4, and $G_i$ is the modulus of rigidity. The latter varies with the material, and depends also upon the magnitude of the deflection of the spring. The last mentioned characteristic is illustrated in Fig. 5, which refers to a particular grade of rubber. For other grades of

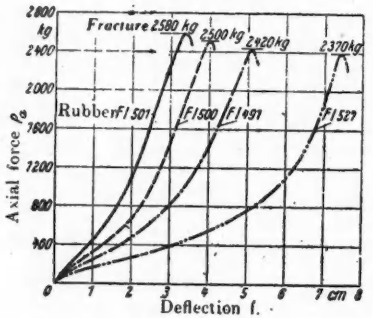


Fig. 2

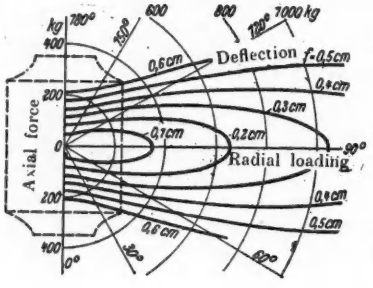


Fig. 3

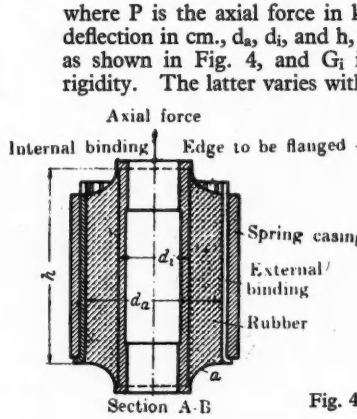


Fig. 4

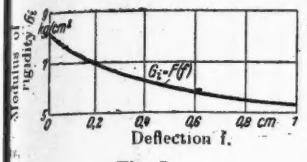


Fig. 5

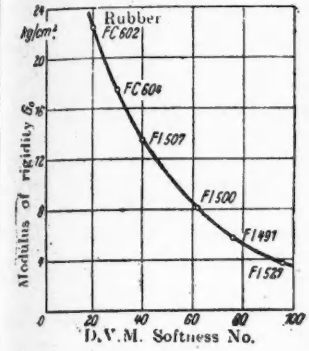


Fig. 6

rubber the curves are of similar shape, but the value of $G_i$ at f=0 is different (Fig. 6). In general, $G_i$ lies between 23 and 3.5 kg/cm² and the more pliable the rubber, the lower its value.

With the aid of formula 1 and Fig. 5 the curves shown in Fig. 7 can be plotted, from which the stiffness at any desired spring deflection can be determined at once. For the same nominal shearing stress intensity

$$\tau_n = \frac{2\,f\,G_i}{d_a - d_i} \quad (kg/cm^2)$$

the spring equation becomes:

$$P = \frac{2\,\pi\,f\,h_a\,G_i}{1 - h_a/h_i} \quad (kg)$$

where $h_a$ and $h_i$ are the height of the outer and inner cylinders respectively.

*Endurance Characteristics.*

The total strength of the spring is composed of two parts, the strength of the rubber spring, and that of the metallic binding. The total strength or durability can be expressed in terms

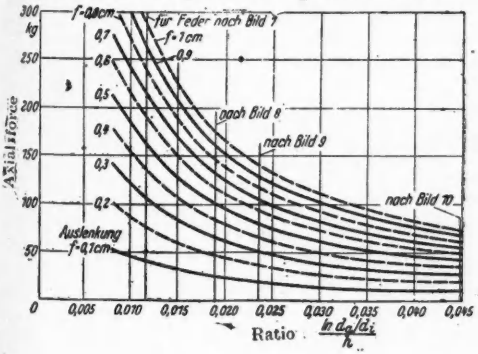


of nominal shear stress intensity, its value depending upon the dimensions, shape, and kind of material of the spring and binding. A good value for this nominal shear stress intensity is 66 kg/cm², and variations are within ± 30%. For the binding material, light alloys give better results than steel.

It was found from practical experience that the temperature of the rubber springs rises to about 80 to 90° C. Investigations have shown that at 85° C the stiffness of rubber springs is 2% less than at room temperature, and at the same time there is a 50% decrease in its durability. The effect of temperature upon these two characteristics is shown in Fig. 8.

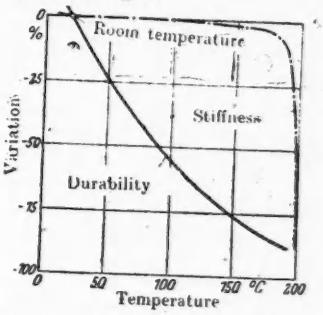


Fig. 8

*Behaviour under a Fluctuating Load.*

In contrast to steel, fatigue failures of rubber springs are not characterised by a sudden breakdown after a specified number of load reversals; instead, a local overheating occurs at some point in the material which becomes glutinous and disintegration follows. The defect then spreads slowly to the surrounding material until a state is reached when the material is considered to be unfit for further service. This condition is reached when the stiffness of the spring has decreased by 10%.

The technique for the determination of the endurance limit of rubber springs is illustrated in Figs. 9-11. Fig. 9 shows the variation of force (for a constant deflection of spring) with the number of reversals denoted by $N_0$-$N_3$. For the sake of comparison the $C_5$ stiffness number was selected as a basis, where $C_n$ stiffness number represents the force that will produce a deflection of n mm. In Fig. 10, the reduction of the $C_5$ stiffness number is shown with increasing reversal from $N_{z6}$ to $10 \times 10^6$. The perimeters $a_1$ to $a_6$ denote spring deflections in increasing order. Finally, we obtain Fig. 11, which is the Wöhler curve for rubber springs. The repetitions are plotted along the abscissae and the ordinates

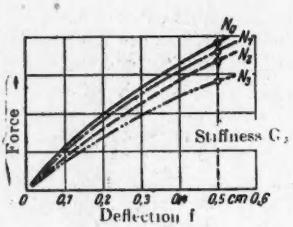


Fig. 9

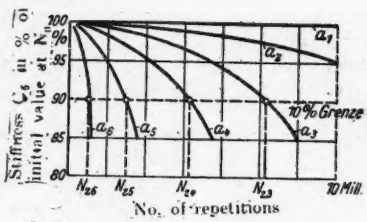


Fig. 10

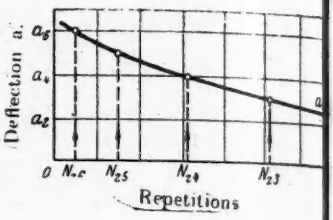


Fig. 11

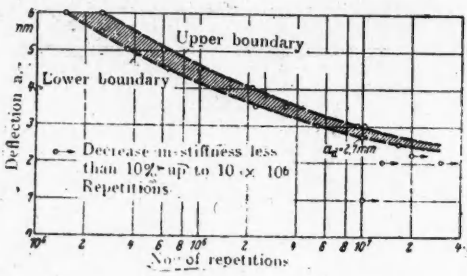
Upper boundary
Lower boundary
Deflection a
Decrease in stiffness less than 10% up to 10 × 10⁶ Repetitions
No. of repetitions

Fig. 12

represent the deflection or amplitude of springing. In practice, the curve is not so clearly defined, but a dispersion of the points will occur (Fig. 12). In this case, for the limiting values of amplitude, points lying on the lower boundary curve should be taken. A striking feature of this graph is that contrary to metals, there is no "limiting range" for rubber, i.e., an amplitude which will not cause failure for infinite service. Therefore, it is essential to specify, in addition to the amplitude, the corresponding number of repetitions.

Table I. gives some data for different types of rubber spring. Spring No. 1 has twice the stiffness of spring No. 3. Therefore, two of the latter could be used in place of spring No. 1. But, as it can be seen from column five, this would mean a reduction of the limiting range (corresponding to $10 \times 10^6$ reversals) of about 33%. A similar comparison can be made in case of collar springs. As a general rule, therefore, smaller springs are inferior to larger ones.

TABLE I.

| Spring type | No. | Volume V cm³ | Specification | D.V.M. Softness No. | Stiffness $C_s$ kg | Endurance limit of deflection mm | Binding |
|---|---|---|---|---|---|---|---|
| 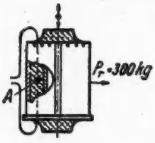 | 1 | 59 | FI 500 | 62 | 172 | ± 2,70 | Rubber on steel |
| | 2 | 59 | Fox 18 | 52 | 240 | ± 2,45 | Buna on steel |
| 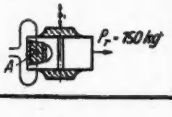 | 3 | 24 | FI 507 | 40 | 86 | ± 1,80 | Rubber on steel |
| 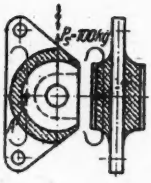 | 4 | 65 | FI 500 | 62 | 110 | ± 1,65 | Rubber on steel |
| | 5 | 108 | FI 491 | 76 | 110 | ± 2,35 | Rubber on light alloy |
| | 6 | 108 | FI 491 | 76 | 110 | ± 2,05 | Rubber on steel |

*) Referred to 10 × 10⁶ repetitions. Frequency n 1000/min A Point of temperature measurement.

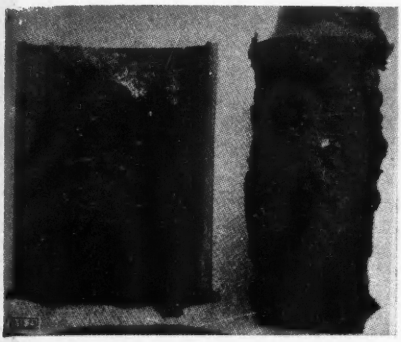

Fig. 13. Failure by Fatigue.

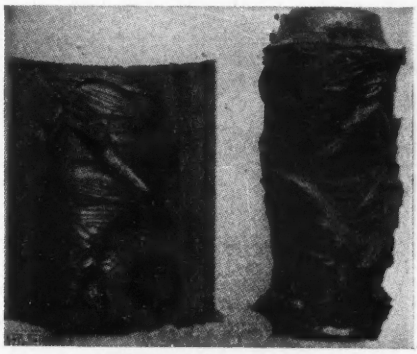

Fig. 14. Ordinary Failure.

*Fatigue Failures and the Effect of Temperature.*

Under the action of a fluctuating load, heat is generated in rubber springs owing to the energy expenditure in damping. This temperature rise is rapid at the beginning, but it reaches a steady value after about ½ to 2 hours. This equilibrium is upset, however, by the onset of fatigue failure. At this stage air enters the inside of the rubber spring at points where the cracks develope. The temperature of the spring will now depend on various ambient factors, such as speed of vibration, air circulation. Naturally, the amplitude of spring deflection will influence the steady value of the temperature in the spring.

As mentioned previously fatigue failure starts with a local overheating which destroys the rigidity of the material, and at the same time the rubber becomes glutinous. That this is a fatigue failure, is obvious, by considering the fact that such failure occurs at deflections which do not cause dangerous temperatures in the spring as a whole. The local overheating starts, as a rule, near, but not in the immediate vicinity, of the metallic binding. The destruction of the material by fatigue takes place on the compression side, while the tension side of the spring shows signs of ordinary failure. The different appearance of the two types of failure is shown by Figs. 13 and 14.

## SYNTHETIC RUBBER FOR SHAFT PACKING

By HANS DIEGMANN. (From *Kunststoffe*, Vol. 31, No. 3, March, 1941, pp. 93-96).

SYNTHETIC rubber is used in many packing applications for motor-cars, aircraft, agricultural machinery, machine tools, etc., replacing chrome leather and felt packings. The high temperature resistance (about 180° C) of synthetic rubber and its resistance to mineral, vegetable, and organic oils, water, glycol, petrol, acids, and bases make it a first class packing material.

Figs. 1 to 5 show synthetic rubber (left) and chrome leather (right) packing rings before and after exposure to heat or chemical attack. In each case the comparison indicates the superiority of synthetic rubber. Synthetic rubber has also the properties of elasticity and flexibility, both of which are important for a good packing material.

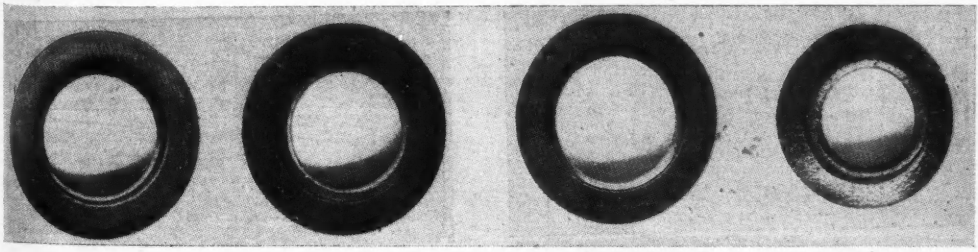

Fig. 1. Original State.

Fig. 2. After 4 hrs. in petrol at 180° C.

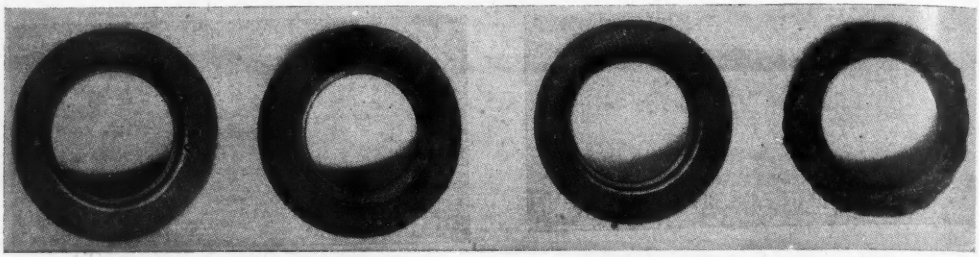

Fig. 3. After 15 hrs. in fuel at 40° C.

Fig. 4. After 3 hrs. in 20% Na OH at 50° C.

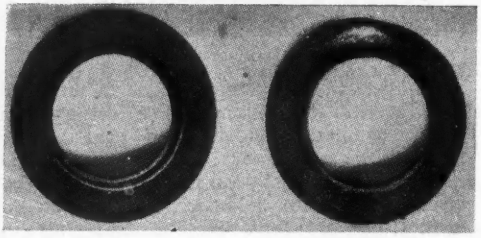

Fig. 5. After 3 hrs. in 20% sulphuric acid at 50° C.

Shown in Fig. 6 is the apparatus for testing packings. A casing comprising a motor driven shaft is fitted with the packings to be tested at the two end plates. The casing is then filled with oil, under pressure if necessary. The casing is free to rotate, and to measure the torque to overcome the packing friction a horizontal beam is attched to it, carrying two scale pans; in this way the torque is determined by balancing the casing.

Fig. 7 shows results obtained by this method. Temperature rise and torque are plotted against shaft diameter. Naturally the temperature rise obtained from this graph will only give indication

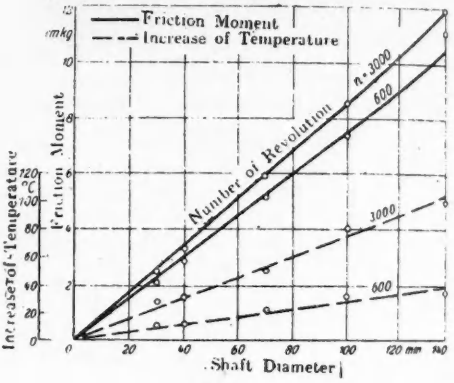


Fig. 7

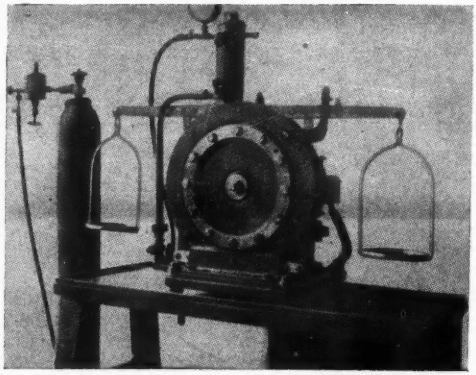

Fig. 6

as to the general behaviour under working conditions; the actual temperature will be influenced by many factors, such as quantity of oil passing through the casing, etc.

Fig. 8 is another comparison between chrome leather and synthetic rubber; the superiority of the latter becomes apparent at once. In general with synthetic rubber as packing material, oils with lower viscosity can be used.

An actual shaft packing is shown in Figs. 9 and 10. The casing (a) is usually made of sheet steel

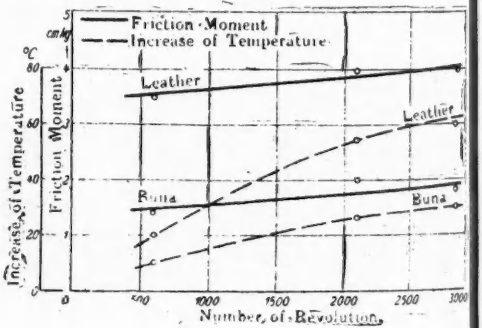


Fig. 8

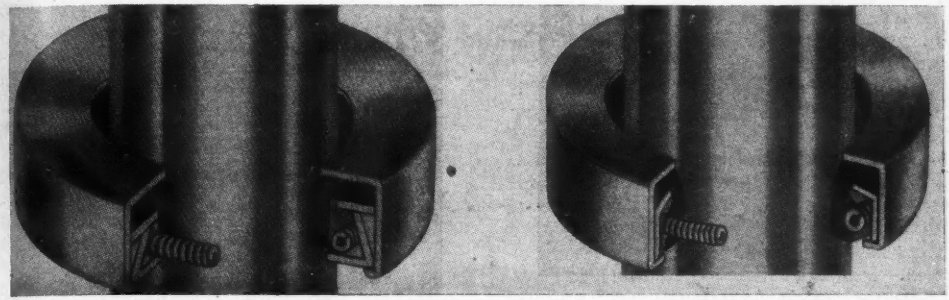

Fig. 9

Fig. 11

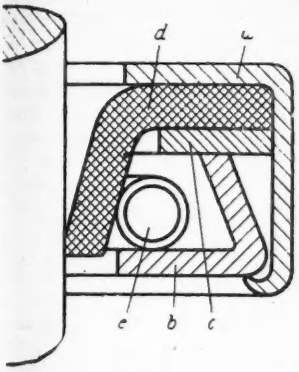


Fig. 10

for deep drawing. Its outer dimension is standardised according to ball bearing standards. The covering ring (b) is made of the same material as (a), is so shaped that the flange pressure is transmitted to the middle of the ring (c) and the packing (d). The synthetic rubber packing (d) should be fixed so that it cannot rotate with the shaft. To reduce heating, i.e., friction, only the outer end of the packing should press against the shaft. Finally (e) is a garter spring which keeps the packing up to the shaft and therefore its proper location is important. Actually the conical shape of the ring (b) keeps the spring in position. The total height of such a shaft gland amounts to about 10-16 mm. Another design is shown in Fig. 11; the width is only about 6-8 mm. and the gland takes up no more space than a simple felt ring.

The proper functioning of such packing rings necessitates careful turning, grinding, and in some cases, polishing of the shaft. The greater the speed, the finer the finish of the shaft must be. The bedding of the packing on to the shaft must be carefully watched, since sharp edges or scoring on the shaft may damage the rubber surface. Naturally the entire packing ring must be prevented from rotating with the shaft.

Packings must always be kept well lubricated. They should never be allowed to run dry, and the better the lubrication the longer its life. The maximum speeds that can be allowed with such packings depend on many other factors, such as air circulation, heat transmissions, etc. In general it can be stated that under normal conditions the life of synthetic rubber packings equals that of roller bearings.

## SUBSTITUTE MATERIALS IN COMPASS MANUFACTURE

By C. LUDKE. (From *Zeitschrift des VDI*, Vol. 85, No. 27, July, 1941, pp. 608-609).

GERMAN engineers are striving hard to counter the serious shortage in some of the manufacturing materials by replacing them with substitute materials. A series of lectures on this subject were held by the VDI, covering Mechanical Engineering and Instruments. Herefrom the present article. [EDITOR].

The navigator's compass is liquid filled to assist in damping out oscillations and vibration. The bowl must be made of a non-ferrous material which does not affect the magnet system. This demand could be satisfied by light alloy, but the liquid used (alcohol and distilled water, volume ratio 1:2) precludes its use because of corrosion difficulties.

New demands made on compasses include the raising of the working temperature limits to $+50°$ C, and $-60°$ C. Within these limits the density of the liquid must be approximately constant to minimize oscillations of the magnet system which must be as dead-beat as possible. The liquid must not become discoloured in course of time, the expansion coefficient should be as small as possible, so as to keep changes in volume during

temperature changes low, and the flash point of the liquid must be high. Most of the hitherto used liquids were unsuitable as far as stability at extreme temperatures were concerned.

Through the medium of co-operation of both the manufacturer and the consumer, a domestic raw material, a petroleum derivative, has been found which is a satisfactory compass liquid. This liquid enables the use of light alloys as well as of synthetic moulded materials for the bowl. By the employment of moulded bowls another difficulty has been encountered in the sealing of the joint glass and between the bowl (Fig. 1), as the expansion coefficient of synthetic resin is about 30 times as great as that of glass. Rubber sealing rings were tried, but these soon became hard at low temperatures and the compass leaked. Rings of Buna have shown themselves superior to anything previously used. Using the new liquid was further advantageous (from the German point of view) as the compass card previously made of mica could be replaced by a light metal card.

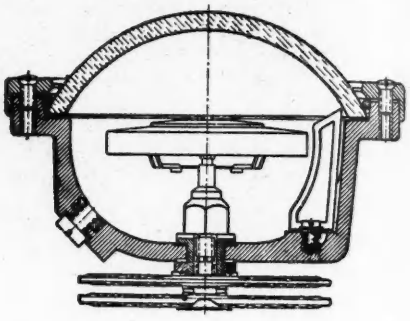

Fig. 1

The required raw material for one compass could be reduced from 4.8 kg to 0.6 kg. The shortage of the particular materials has been thus eliminated.

## STRESSING OF LORRY CHASSIS FRAMES

By Prof. Dr. A. Thum and Dipl. Ing. A. Erker. (From *ATZ, Automobiltechnische Zeitschrift*, Vol. 44, No. 7, April, 1941, pp. 167-170).

The chassis frame of lorries and trailers consists generally of two long girders connected by two or more lateral beams. To-day, the stressing procedure of such a frame is universally limited to the calculation of the bending moment on the longerons when the frame is stationary on a horizontal, even road, and under the action of a uniformly distributed load.

To cater for additional loads due to acceleration encountered in driving, an " impact allowance " of 40% is being made. With these assumptions, a maximum stress between 10 to 14 kg/mm² (about 14,000 to 20,000 lb/sq. in.), which is regarded as allowable, should be just reached.

The frequency of springing or distribution of loading is thus left out of consideration, and many fractures have occurred which could only be explained as fatigue fractures.

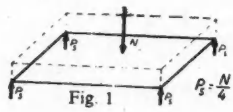


Fig. 1

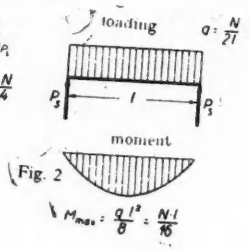


Fig. 2

N = Resultant of load
$P_s$ = Wheel load

### Various Cases of Loading.

To get a clear picture of the different stresses and their probable frequency, the various cases of loading will be considered. The frame under consideration is simplified, consisting of two longerons and two lateral beams.

### Stationary Vehicle on an Even, Horizontal Road.

This case is illustrated in Figs. 1 and 2. The wheel loads are equal in magnitude and direction; the case being that of symmetrical loading. The maximum bending moment is used for the dimensioning of the beam.

### Stationary Vehicle on an Uneven Road.

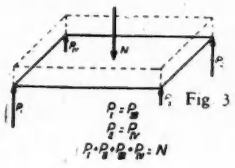


Fig. 3

In this case the wheel loads are not equal (Fig. 3). For reasons of equilibrium and symmetry the wheel loads of each pair of wheels

diagonally opposite are equal. This general case of loading can be thought composed of two cases of loadings, namely that of the symmetrical loading shown in Figs. 1 and 2, and that shown in Fig. 4 defined in the following as asymmetrical loading. By definition, asymmetrical loading yields wheel loads of equal magnitude, but of opposite direction for neighbouring wheels.

By superimposing the asymmetrical loading on the symmetrical loading, the case may be that of Pa=Ps=N/4, when only two wheels are loaded, the two others, as shown in Fig. 5, carry no load at all, i.e., are lifted up from the road. This represents the most unfavourable case of loading for a stationary vehicle on uneven road.

**Driving over Obstacles, Taking Bends, etc.**

The two cases of loading described above for stationary vehicles on even and uneven road can also be obtained when the vehicle is in steady motion. Accelerations of short duration, as those for instance caused by an obstacle lifting the front axle (both wheels an equal distance), however, increase the bending moment to the side of the lifted axle as shown in Fig. 6. The annotation being: N=dead load + useful load, M=N + impact forces, P=load on wheel due to N, Pb= impact force due to acceleration.

The same notation and the same reasoning is contained in Fig. 7, showing the bending moment for the case of impact on a single wheel.

When taking a bend the outer side of the chassis becomes more heavily loaded due to centrifugal action. In addition, torsion of the frame causes a further modification of the loading.

Generally speaking, great changes in the distribution of bending moments are due to braking. Uneven braking of opposite wheels introduces forces in the plane of the frame.

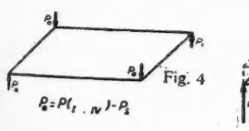
Fig. 4

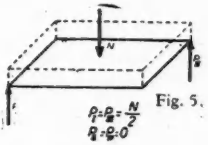
Fig. 5.

Fig. 6

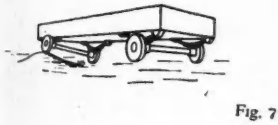
Fig. 7

**Bending and Torsion of the Frame.**

Pure bending of the longerons, for which symmetrical loading is responsible, presents no difficulty. The asymmetrical loading, however, represents a redundant system, the solution of which requires a somewhat more laborious calculation.

The simple frame chosen for illustrating the problems can be made statically determinate by cutting for one member, e.g., of member II.-III. in Fig. 8. At the point of separation generally six unknowns can be introduced:

(1) A longitudinal force in direction (x).
(2) A lateral force in direction (y).
(3) A lateral force in direction (z).
(4) A bending moment in the x-y plane.
(5) A torsional moment in the y-z plane.
(6) A bending moment in the z-x plane.

Of these six values some become zero at the chosen point. In the cut frame no longitudinal forces can be acting, and likewise, no shearing forces and moments in the plane of the frame. Keeping in mind the deformation of member II.-III. under torsion (Fig. 11), it can be seen that the bending moment in the x-y plane disappears. There remain:

(1) The lateral force in direction (y) (Fig. 9).
(2) The torsional moment in the y-z plane (Fig. 10).

By solving the appropriate equations of elasticity, the final stresses and deformations of the frame can be calculated (Fig. 12).

**Torsion and its Influence on various Beam Cross-sections.**

Calculations were made for these cross sections of approximately equal modulus of section. The beam depth and the total dead load was in all cases the same.

As the result, the following values are given in Table I.:

(1) The load carrying capacity (N).
(2) The maximum asymmetrical load $P_{max}$ for theoretically most unfavorable loading.
(3) The torsional rigidity of the frame CT, expressed as force required to twist the end-beam against the head-beam by one degree.
(4) The stress parameter KT, expressed as the maximum "equivalent stress" (according to combined bending and twisting) prevalent at a twist of one degree of the end-beam against the head-beams.
(5) The maximum stress at maximum asymmetrical loading (equivalent stress max.).
(6) Angle of twist $\beta^{o}$ at maximum loading of the end-beam against the head-beam.

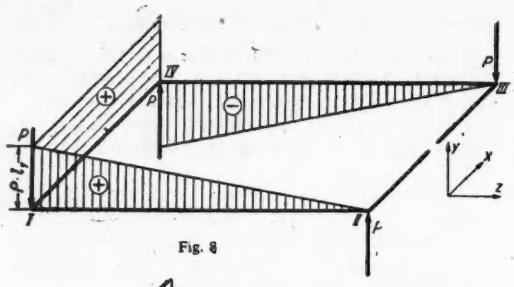


Fig. 8

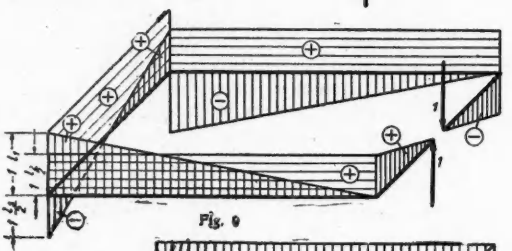

Fig. 9

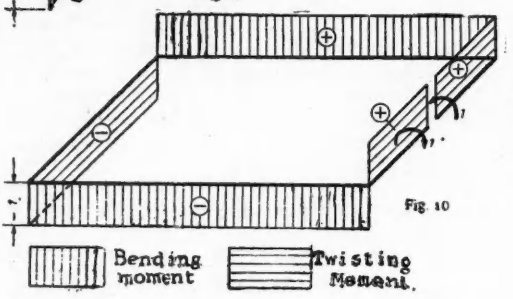

Fig. 10

Bending moment

Twisting Moment

(7) The strain energy E necessary to produce an equivalent stress of 1000 kg/cm² (14223 lb/sq. in.).

Each of the frames A and B differ only by the head-beam, which in case B is very rigid as shown by thick lines. The ratio of length to width (L:B) was 2:1 and 5:1.

Column 5a gives $\sigma_{gw}$, the probable maximum stress was not coincident with $\sigma_{g\ max}$. In these cases the theoretical maximum stress cannot be developed, as the springs take a great part of the deformation which otherwise in the absence of springing would result in a torsional deformation of the frame. With increasing ratio of L:B, however, even the practical stresses reach a dangerous value, which when frequent, can lead to fatigue failure. The only sections not prone to failure are box and tubular. For the latter, especially the stresses due to torsion, are always low. Under impact the box beam is the more favorable, having the highest strain energy value.

**Torsionally Weak and Torsionally Rigid Frames.**

In designing frames weak in torsion, care must be taken that all members of the frame be equally elastic. Parts of greater rigidity, e.g., rigid head-beams, or stiff mountings, such as those for spare-wheels, etc., create unfavorable stress distribution. In cases where a torsionally weak frame is connected to a rigid member it may happen that the member takes the whole torsion, for which it has not been designed. At higher speeds, for this type of frame, there is danger of flutter.

Frames rigid in torsion are less liable to flutter, also the constancy in stiffness of the members is of less importance. However, the most suitable type of frame cannot generally be stated, as matters of economics, design, and springing, have to be taken into account.

**Riveting or Welding.**

In connection with the stiffness of the frame it is of great interest as to whether riveting or welding should be employed.

Welding offers success with frames torsionally rigid, as welded joints are more rigid than riveted ones. Every care should be taken to avoid welding notches as these reduce the fatigue strength. To this end welds should be ground.

For torsionally weak frames the greater elasticity of riveted joints is often of advantage. The excellent service of these frames is greatly due to riveting, which is less liable to aggravate design faults as is the case with welded joints.

Fractures, however, have shown that there is

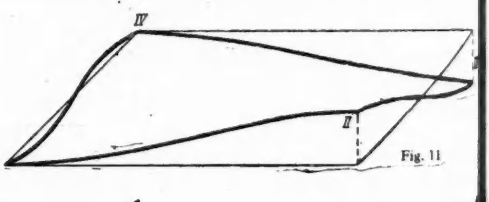

Fig. 11

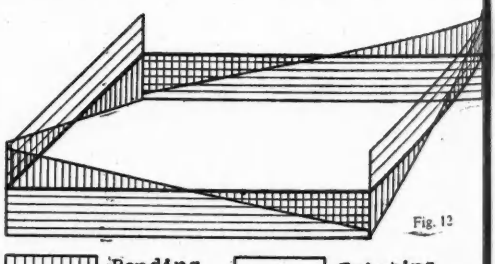

Fig. 12

Bending Moment

Twisting Moment

no absolute safety against excessive stresses due to torsion. If higher safety is desired the rigid frame only can offer it. In lorry design it seems, therefore, advisable to develop the rigid frame further, especially in conjunction with rigid bodies (buses).

TABLE I.

| Frame | Cross section of beam | 1<br>N<br>kg | 2<br>$P_{max}$<br>kg | 3<br>$c_T$<br>kg<br>1 ° | 4<br>$k_T$<br>kg/cm²<br>1 ° | 5<br>$\sigma_{gmax}$<br>kg/cm² | 6<br>$\beta$<br>° | 5a<br>$\sigma_{gw}$<br>kg/cm² | 7<br>E<br>kg cm<br>1000 kg/cm² |
|---|---|---|---|---|---|---|---|---|---|
| I A | ⌞ | 6900 | 1700 | 12 | 130 | (18500) | (140) | 1470 | 630 |
| | □ | 5600 | 1400 | 620 | 540 | 1200 | 2,24 | — | 1830 |
| L:B = 2:1 | o | 5350 | 1350 | 1690 | 1100 | 870 | 0,79 | — | 1230 |
| I B | ⌞ | 6900 | 1700 | 880 | 2000 | (3900[1]) | 1,95 | — | 190 |
| | □ | 5600 | 1400 | 990 | 1680 | 2400 | 1,41 | — | 300 |
| L:B = 2:1 | o | 5350 | 1350 | 2080 | 1680 | 1050 | 0,64 | — | 640 |
| II A | ⌞ | 5500 | 1400 | 15 | 100 | (9000) | (90) | 2350 | 630 |
| | □ | 4500 | 1130 | 810 | 420 | 590 | 1,39 | — | 1950 |
| L:B = 5:1 | o | 4300 | 1080 | 2300 | 850 | 390 | 0,47 | — | 1400 |
| II B | ⌞ | 5500 | 1400 | 130 | 340 | (3700*) | 10,9 | — | 480 |
| | □ | 4500 | 1130 | 900 | 590 | 730 | 1,24 | — | 1140 |
| L:B = 5:1 | o | 4300 | 1080 | 2420 | 880 | 390 | 0,44 | — | 1360 |

* Particularly highly stressed frame.

## IMPACT STRENGTH OF PRE-STRESSED SPECIMENS

By S. I. BELOSTOTSKY. (From *Závodskaja Laboratoria, Moscow*, Vol. 10, No. 2, 1941, pp. 186-190).

THE behaviour of materials under a combination of static load and impact has never been deeply investigated, probably owing to the many unsatisfactory features of impact tests, namely the fact that laws of geometric similarity are not applicable as between different sizes and shapes of specimens, the lack of consistency of the results obtained, even with identical specimens, and the imperfect understanding of the physical meaning of impact strength "toughness" test figures, which precludes their introduction into engineering formulæ. This leads many engineers to regard impact testing as too empirical for scientific research, but it can nevertheless be made to yield interesting results.

In the series of tests described below the first concern was to devise test conditions which would permit of imposing and measuring simultaneous static and dynamic loads with specimens which would be uniform in size, shape, and quality, and yet available in large quantities without undue expense. After numerous preliminary experiments the following procedure was adopted.

For combined static and dynamic bending two materials, described in the Table as No. 1 and 2, both being steels, but of widely different quality, were used. Steel No. 1 of high tensile strength gave a straight, crystalline fracture and absorbed little energy when failing by impact. Steel No. 2, on the other hand, of lower tenacity but more

ductile, absorbed a relatively large amount of energy at impact and showed the characteristic dull, conchoidal fracture with local extension at the plane of failure.

The form of specimen adopted for the above tests is shown in Fig. 1a, and it will be seen that it is a round bar 5 mms. diameter with a square notch 1 mm. deep and 1 mm. wide, i.e., the Fremon type of notch. This specimen was inexpensive to produce, easy to fix, and it jumped clear of the pendulum after fracture. If it were not for the limited means at the disposal of the laboratory, however, tests would have been carried out on specimens of larger diameter, in order to get greater resistance to impact, and lessen the effect of such factors as grain size and minor defects in the material.

Fig. 2 shows diagrammatically how static bending moments were applied, and Fig. 3 illustrates the application of static tension, the specimen in the latter case being as detailed in Fig. 1b.

TABLE II.

MATERIALS SUBJECTED TO COMBINED LOADING TESTS.

| No. | Type of Load | Material | Diam. mms. | Tenacity kg/cm² | % Elong. | Spec. impact resist. kg/cm² | Area cm² | Nett working area cm² | Shape |
|---|---|---|---|---|---|---|---|---|---|
| 1 | Static and dynamic bending | steel rod | 5 | 11.000 | 8 | 6 | 0.2 | 0.17 | Fig. 1a |
| 2 | ditto | ditto | 5 | 6250 | 6 | 13 | 0.2 | 0.17 | ditto |
| 3 | Static Tension and dynamic bending | Wire | 3 | 11.430 | 5 | 6 | 0.07 | 0.063 | Fig. 1b |
| 4 | Static tension and perpendicular blow | ditto | 0.9 | 9000 | 6 | very high | 0.0064 | 0.013 | Wire bent double |

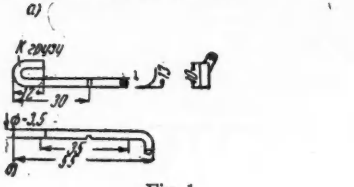


Fig. 1

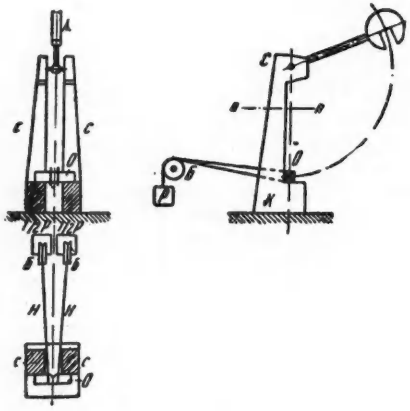

Fig. 2

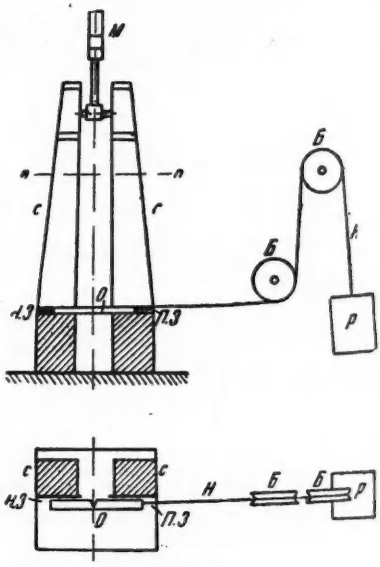


Fig. 3

Two pendulum testing machines were used: an Amsler type of 15 kg-metres maximum energy and a Charpy of 1.5 kg-m.

The apparatus was carefully checked, and tables were compiled of energy losses due to air resistance, bearing friction, etc., and while it is impossible to enumerate here all the precautions taken to ensure accuracy, it may be mentioned that particular attention was given to preventing obstruction of pendulum motion by the specimen itself after fracture; it was found that even contact with the loose end of a wire could affect the reading. All experiments were conducted at an even temperature of 10-15° C, and the use of two different testing machines gave an opportunity for cross-checking results.

The experiments were conducted in such a way as to give results which could be plotted in the form of a diagram. Figs. 4 and 5 show the type of loading applied. The directions of the static and dynamic efforts relative to the specimen correspond to the four quadrants of the diagrams, while their numerical values are the co-ordinates of a series of points through which a smooth curve can be plotted.

The utility of plotting the actual experimental values obtained in this way is open to question, of course, and arguments could be brought forward

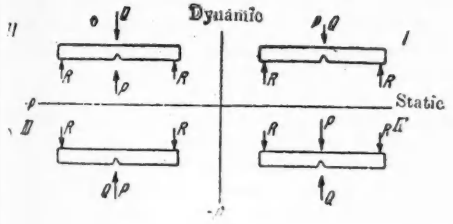


Fig. 4

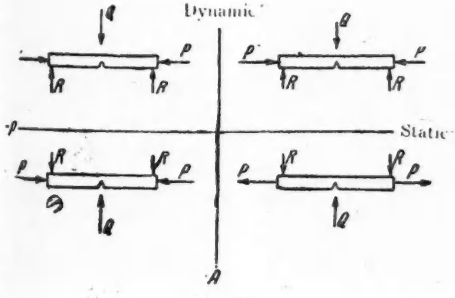


Fig. 5

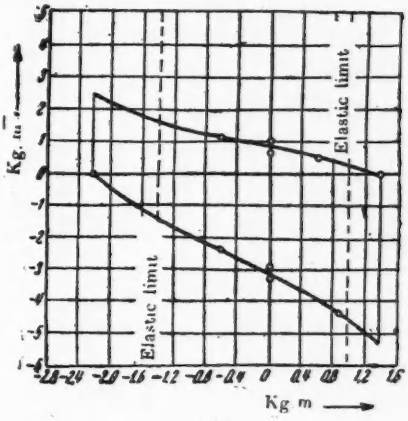


Fig. 6

in favour of working out the relation between "specific toughness" and the static stresses, or between the static and dynamic stresses involved. But since impact test figures, in any case, do not comply with the ordinary laws of geometric similarity, there appeared to be little gain in going through a long series of calculations which would obscure rather than clarify the picture. It was decided, therefore, to plot simply the actual test figures in the form of

$$A_{dynamic} = F(P_{static})$$

After a great deal of preliminary work in the way of tracing and eliminating the causes of discrepancies between individual readings, it was possible to obtain consistent results without undue scattering of points. These were then plotted to a large scale on the principle of the "weighed average" and smooth curves were drawn, which may well be described as "diagrams of failure under combined loading."

Typical curves of this nature are given in Figs. 6, 7, 8, and 9. In each case a few of the experimental points have been retained to indicate the extent of their dispersion.

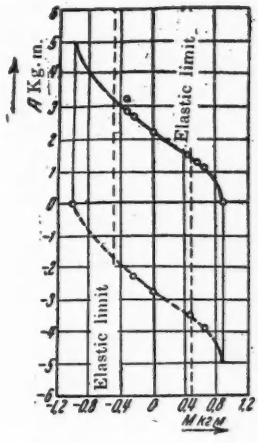


Fig. 7

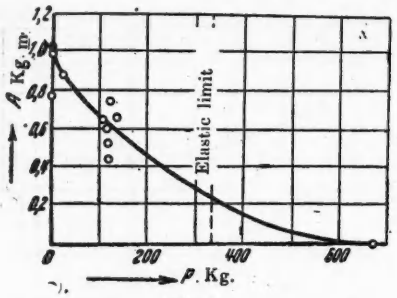


Fig. 8

It should be noted that in quadrants II. and III., the specimen tends to behave in accordance with Davidenko's dictum that "specimens of tough ductile steel cannot be broken by bending unless notched," and therefore, the energy of failure recorded in this case is not that of actual fracture but of bending to such an angle that the specimen slips out between its supports. To avoid misunderstanding the corresponding part of the diagram in Fig. 7 is shown dotted.

When working with wire specimens (Fig. 9) this was used doubled up, but not twisted together.

The curves given here, as well as a great number of others obtained in the laboratory, fully justify a general classification of all such diagrams, so far as Quadrant I. is concerned, into three main types illustrated in Fig. 10. It will be seen that the curve is bulged upwards for "tough" materials and downwards for brittle ones.

With ductile materials, in other words, small static loads have scarcely any effect on resistance to impact ($A_1$ is very small) while greater loads decrease impact strength at a sharply increasing rate, making the material brittle ($A_2$ rapidly increases with P).

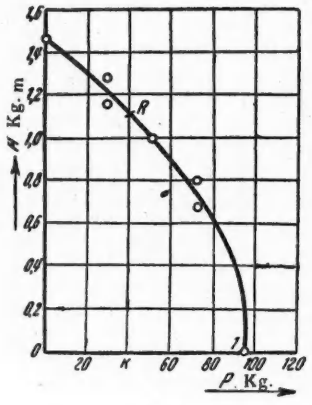


Fig. 9

With brittle materials, on the other hand, even a small static load causes a great reduction in impact strength, and this effect becomes relatively less pronounced as the static load

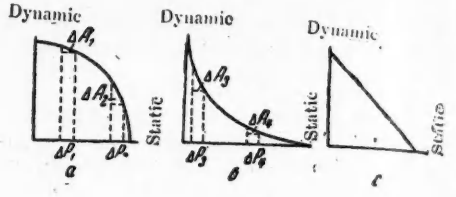


Fig. 10

increases and impact strength becomes very small In the case of materials such as chrome-nickel steel, which are equally capable of resisting static and dynamic loading, it is reasonable to expect an intermediate type of "diagram of failure" as represented by Fig. 10c.

In a similar way Quadrants II. and IV. of our diagrams can be used to illustrate the increase in impact strength consequent upon favourable static loading.

The experiments described above may be regarded as a first step in the direction of testing materials for combined static load and sudden heavy impact. It would appear most desirable that:

(1) Special apparatus should be brought out for the specific purpose of such combined testings: the particular laboratory installation is shown in Fig. 11 with detail of tension attachment in Fig. 12.

(2) Diagrams of failure for various materials should be obtained in all four quadrants, and the possibility of introducing their conclusions into practical design calculations thoroughly investigated.

The practical importance of the questions raised cannot be disputed since combinations of static loads and shock occur in most important structures and machine elements. It is essential, therefore, to find out how materials of construction behave under such combined stresses.

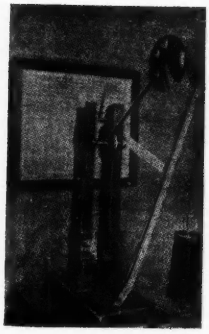

Fig. 11

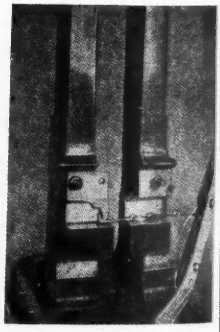

Fig. 12

# MEASUREMENT OF PHOTO-RECORDING OF MAGNETOSTRICTION BY THE KORNEZKY METHOD

By Y. P. SELISSKY. (From *Závodskaja Laboratoria, Moscow*, Vol. 10, No. 4, 1941, pp. 382-385).

THE measurement of magnetostriction of a ferromagnetic alloy is of considerable interest because it is one of its fundamental characteristics. Nevertheless, the choice of methods, in practice, is not large, the best known being :

(1) The optical lever method of what might be termed the Japanese school headed by Prof. Honda (S. Kaya, I. Masuyama and Z. Nishiyama).

(2) The variable capacity method, as adopted by Lichtenberger, Schulze, and others.

The drawback of the former is its relatively poor sensitivity, which is particularly objectionable for small values of magnetostriction. The alternative method, on the other hand, involves an elaborate electrical installation, and practical difficulties with the attachment of condenser plates to the specimen.

M. Kornezky, in his research on the volumetric magnetostriction of iron (see *Zeit. f. Phys.*, 87, 563, 1934), has modified the Japanese method in such a way as to obtain greatly improved sensitiveness, and it is this modified method that was adopted in the Union Electrical Institute for research work on ferro-magnetic alloys by A. Zainovsky, A. Pedko, and the writer. Later, the writer constructed an apparatus permitting of automatic recording of magnetostriction values on sensitised paper. The complete installation, therefore, was as follows.

Referring to Fig. 1, 0 is the specimen (6 mm. diam. and 200 mm. long), located inside a copper container-tube P in such a way that one end of it is pressed against the copper plug H by rubber bands while the other end passes freely through the copper ring K.

The indicating system consists of aluminium rods $C_1$ and $C_2$ joined together by a bronze spring S and having wolfram needle-points at their free ends. The needle-point of $C_1$ rests on a jewel bearing glued to the specimen, while that of $C_2$ lies in a similar bearing mounted in the screw B. The rod $C_2$ has a branch $C_3$ which protrudes through a slot in the container tube, and between this branch and a guide-plate E, is located the spindle A on which is mounted a small, rotating, mirror, 3. The weight of the little mirror is balanced by a counterweight, W.

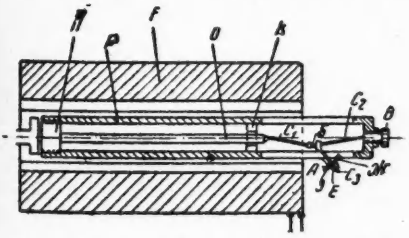

Fig. 1. The Kornezky apparatus for measuring magnetostriction.

By turning the screw B, the spring S is loaded and rods $C_1$ and $C_2$ take up a slight angle. The load on the bearings, however, is very small, so that the mechanism is not jammed, but rotates freely until its weight comes to bear on the spindle of the mirror.

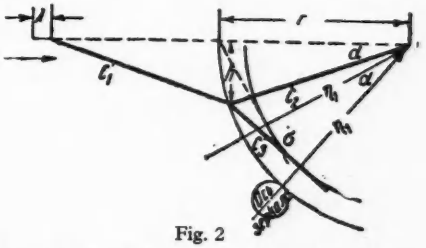

Fig. 2

The velocity ratio, or magnification effect, of the mechanical part of the system is readily arrived at by reference to Fig. 2. The rods $C_1$ and $C_2$, which are originally in line (as shown dotted), are compressed by the amount $\lambda$, and take up a position shown by thick lines with a sideways departure of "h." If now magnetostriction produces a change in the length of specimen equal to $d\lambda$, the point of contact of $C_3$ with the spindle of the mirror will move by an amount $d\sigma$ along an arc of radius r, and the velocity ratio will be:

$$U = \frac{d\sigma}{d\lambda} \quad .. \quad .. \quad .. \quad .. \quad (1)$$

From Fig. 2 it will be seen that

$$h^2 + \left(\frac{2r-\lambda}{2}\right)^2 = r^2$$

$$\lambda - 4r\lambda + 4h^2 = 0$$

$$\frac{\lambda^2}{4r^2} - \frac{\lambda}{r} + \frac{h^2}{r^2} = 0$$

$$\frac{h}{r} = \sin\alpha \; ; \; \alpha = \frac{\sigma}{r}$$

Hence:

$$\sin\frac{\sigma}{r_1} = f\left(\frac{\lambda}{r}\right)$$

$$-\sin\frac{2\sigma}{r_1} = \frac{\lambda^2}{4r^2} - \frac{\lambda}{r}$$

Differentiating with respect to $\lambda$

$$-\frac{2}{r_1} \times \frac{h}{r}\cos\frac{\sigma}{r_1} \times \frac{d\sigma}{d\lambda} = \frac{2\lambda}{4r^2} - \frac{1}{r}$$

or, $$\frac{\lambda}{2r} - 1 = -\frac{2h}{r}\cos\frac{\sigma}{r_1} \cdot \frac{d\sigma}{d\lambda}$$

$$\frac{d\sigma}{d\lambda} = \frac{r_1}{2h}\left[\frac{1}{\cos\alpha}\left(\frac{\lambda}{2r} - 1\right)\right] \quad .. \quad ..(2)$$

From Fig. 2 it will be clear that:

$$\frac{2r - \lambda}{2} = r\cos\alpha$$

And substituting this in equation (2) we finally get

$$U = \frac{d\sigma}{d\lambda} = \frac{r_1}{2h} \quad .. \quad .. \quad .. \quad (3)$$

This, of course, applies only to small changes in the length of the specimen.

In our experiment the initial "h" was invariably set at 2 mms. and was measured with the aid of a microscope micrometer.

The change in position of $C_3$, causes a rotation of the axis of the mirror and, therefore, by focussing a light on the mirror and reading the position of the reflected spot of light on a graduated scale, the magnetostriction can be measured with a high degree of magnification and accuracy.

To calculate the full overall magnification, take L, = 3280 mms., the distance from mirror to the graduated scale; S the distance traversed by the spot of light along the scale; $\rho = 0.25$ mm., the radius of mirror spindle and $\psi$ the angular movement of the spot of light. Use the symbol $\lambda$ to represent the unstrained length of the specimen (200 mms.), leaving $d\lambda$, as before, to represent its change of length due to magnetostriction, and $d\sigma$ the movement of $C_3$, which being small, can be regarded as in a straight line.

Then $S = L \cdot \tan\psi$

and, because $\rho$ and $d\sigma$ are small, we can write

$$d\sigma = \rho\tan\psi$$

$$S = L\frac{d\sigma}{\rho}$$

$$d\sigma = \frac{\rho}{L}S$$

But from (1) $d\sigma = Ud\lambda$

So that $$\frac{\rho}{L}S = Ud\lambda;\ d\lambda = \frac{\rho}{U.L}S$$

Therefore magnetostriction per unit length

$$\frac{d\lambda}{\lambda} = \frac{\rho}{UL\lambda} \cdot S = \frac{0 \cdot 25 \times S}{10 \times 3280 \times 200} = 3 \cdot 8 \times 10^{-8} \cdot S$$

In other words 1 mm. on the scale represents an extension of

$$d = 3 \cdot 8 \times 10^{-8} \times 200\,\text{mm} = 76 \times 10^{-7}\,\text{mm} = 76\,\text{Å}$$

(7·6 millionths of a millimeter).

The recording of test figures was expedited by arranging that the spot of light should fall on photographic paper in such a way as to obtain in one operation all the data for a complete magnetostriction curve $d\lambda = f(H)$, when H is the magnetic field. This apparatus is shown diagrammatically in Fig. 3. K is the magnetising coil with its copper tube containing the specimen, and the current is supplied from the two-way switch C through a rheostat R.

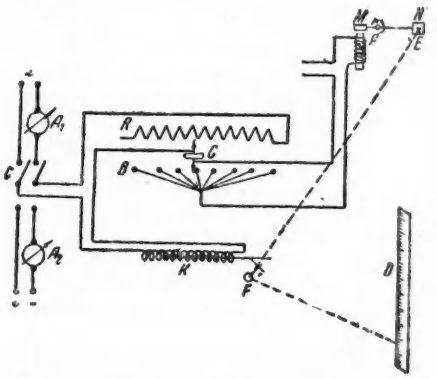


Fig. 3. Diagrammatic arrangement of apparatus for photo-recording of magnetostriction.

The rheostat is made up of three sections in series, all of Ni-Cr wire of the same gauge, wound on the same former. The first section is of single wire, however, while the second consists of two wires in parallel and the third of four. This construction makes it possible to vary the current from 0.1 to 8.0 amps very smoothly. The magnetising current is supplied by a 120 volt accumulator, and a 220 volt A.C. supply is used for de-magnetising.

By the side of the rheostat R is a panel B with

a series of contacts which are connected with a relay circuit, and the rheostat slider, G, is arranged so that its upper end touches these contacts in the course of its travel, thus making and breaking the relay circuit.

When the relay coil, P., is energised its core pulls down a little weight, M, mounted on one end of a lever, thereby lifting the shutter, N, mounted at its other end. This uncovers the source of illumination, E, so that a ray of light falls on the movable mirror, F, and is reflected to the graduated scale, D, or on a strip of photographic paper.

The position of the contacts corresponds to definite values of magnetising field, varying from 18 to 870 units. And as the slider, G, touches consecutively the several contacts, so the corresponding positions of the spot light is recorded on the sensitised paper. The result is a photographic record (shown by the narrow strip at the extreme left of Fig. 4) from which the amount of magnetostriction can be calculated for a number of known values of magnetic field strength. It can also be used very conveniently for direct construction of a magnetostriction curve of the form $S = f(H) = \frac{d\lambda}{3 \cdot 8}$ as shown in Fig. 4. The example actually chosen in the illustration is of an alloy of positive magnetostriction.

The apparatus described is extremely sensitive, permitting measurement of magnetostriction of the order of $10^{-6}$ within 4%. The actual accuracy during our experiments was somewhat lower owing to certain adverse influences, amongst which may be mentioned variations in the supply voltage, small temperature changes, and mechanical vibrations. However, the time of obtaining the complete record of $d\lambda = f(H)$ for one specimen does not exceed 5 seconds, so that the incidence of temperature changes and mechanical vibrations (which tend to alter the zero position) is reduced to practically negligible proportions.

After one series of points has been recorded, the specimen can be de-magnetised with alternating current and the experiment repeated if deemed necessary.

The field inside the coil is not altogether uniform, being about 80% as strong at the ends as in the middle. This may be disregarded, however, in cases where the main point of interest is the magnetostriction of saturation.

The performance of the apparatus was checked against a standard specimen of electrolytic nickel. The curve of $\frac{d\lambda}{\lambda} = f(H)$ for this specimen, without correction for de-magnetising factor, is given in Fig. 5. If the curve of magnetostriction has a maximum or minimum point (e.g., iron) then the recording must be done in two operations.

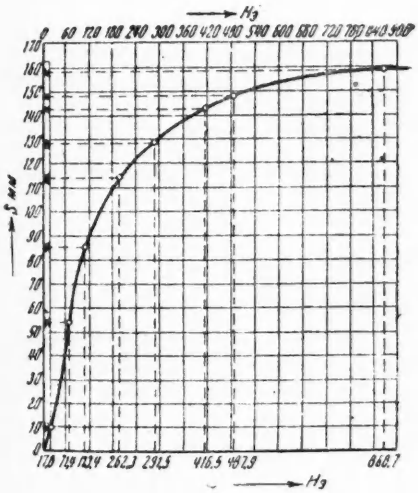


Fig. 4. Illustrating the use of a photo-record for constructing a magnetostriction curve.

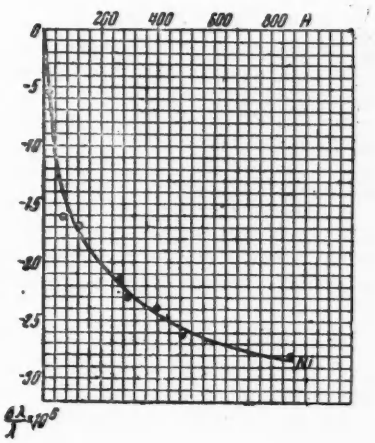


Fig. 5. Magnetostriction curve for standard specimen of electrolytic nickel.

# THE USE OF FLUORESCENT MATERIALS FOR LIGHTING PURPOSES

By WERNER A. SEELIG, Berlin. From *Elektrotechnischer Anzeiger*, Vol. 58, No. 7, April 2nd, 1941, p. 206/10. (*Continued from page* 361.)

THE ultra-violet radiation is diffused by an enamelled steel reflector and renders the luminescent paints fluorescent as shown in Fig. 2. Even inscriptions can be rendered legible, as can be seen from this figure.

Other new uses will be developed in peace time, e.g., the painting of buildings situated in streets without general illumination, like filling stations outside of towns and villages. Energy consumption of such lighting installations is low, as one HQV 500 lamp has a consumption of 130 Watt, losses in the choke coil included.

## Use of fluorescent materials for lamps for general illumination.

*Hg-high-pressure lamps with fluorescent coating.*

When the inner surface of the discharge tube or of the enveloping glass is coated with fluorescent material, the radiation passing this surface assumes a colour depending on the chemical composition of the coating. The first type of such a source of light was the so-called HgL-lamp, which is in regard of its electrical design identical with the well-known HgQ-lamp with an output of 3,300 or 5,500 Hlm. The only difference consists in the use of a larger glass bulb in order to be able to apply a great quantity of fluorescent material in a coating not too compact. The unavoidable restriction of the quantity of the fluorescent material had the consequence that the colour of the light could not be made very intense. One had to do without bringing the colour of the light very near daylight. Therefore the fluorescent lamp has been used often together with incandescent lamps in the well-known manner. But it seems that these lamps will find extensive use for outdoor illumination after the war, as they do not introduce disagreeable changes of the normal colours.

*Hg-low-pressure lamps with fluorescent materials.*

In order to design a light source suitable for all purposes based on the principle of fluorescence it was necessary to use larger fluorescent surfaces. As that could not be achieved with the Hg-high-pressure discharge lamps, the Hg-low-pressure lamp has been applied, the first Hg discharge light source introduced in practice about 30 years ago. Of course, the Cooper-Hewitt lamp of this period has undergone a complete transformation meanwhile, especially by the introduction of a new type of electrodes, which gave the lamp a longer life, better ignition and higher efficiency. There exist at present two types of fluorescent tubes, the one using high tension current like the tubes used for advertising, the other working with 220 V like the high pressure lamp and the Cooper-Hewitt lamp.

The high tension fluorescent tubes are manufactured with a standard length of 2 m and connected to a transformer with a secondary voltage of 1 to 3 kV, or single or several in series. The following table illustrates the working conditions of these high tension tubes:

TABLE I.

| Type of lamp | Colour | Intensity of current | Energy input | Luminous flux | Photometric efficiency |
|---|---|---|---|---|---|
| Hg NL 35 250 ro | reddish-white | | | | Dia. of tube 35 mm. |
| | | 250 mA | 65 W | 2200 Hlm | 34 Hlm/W |
| Hg NL 35 250 | daylight white | | | | |

From 2 to 18 m. tube can be fed from one transformer. At temperatures below 18° C a higher voltage is necessary than at higher temperatures. Therefore the voltage applied has to contain some reserve. In regard of the high voltage used for these lamps the installation has to be made with great care. An automatic breaker has to be provided, which disconnects the lamps, when one or several tubes are not in order. Two colours can be produced with these lamps: "Technical daylight" and a reddish-white coloured light, which is very suitable for reception rooms and so like.

For the same colours lamps working from low voltage distribution have been designed. These lamps (Fig. 3) have a very high efficiency, given in Table II.

TABLE II.

| Type of lamp | Colour | Intensity of current | Energy input | Luminous flux | Photometric efficiency | Diam. of tube |
|---|---|---|---|---|---|---|
| HNT 100 | daylight white | 0.25 A | 28 W | 1100 Hlm | 39 Hlm/W | 35 mm. |

These lamps will be successfully used where light of daylight colour is necessary, as in the paper and textile industry. The installation is very simple, if the accessory apparatus are placed in the casing of the lamps. Applying the same fluorescent materials as for the high voltage fluorescent lamps one can design low tension fluorescent lamps too, which give a reddish-white light containing a more intense red and blue radiation than that of incandescent lamps.

## BAND-VISCOSIMETER

By DR. F. WACHHOLTZ. (From *Die Chemische Fabrik*, Vol. 14, No. 8, April, 1941, p. 155).

A NEW addition to measuring instruments is the band-viscosimeter designed to investigate the influence of suspended pigments in oils, and which has since proved to be a valuable means of determining the viscosity of viscous fluids and pastes.

The band-viscosimeter consists essentially of two metal blocks with rounded up corners. A gap between the blocks is maintained by thin gaskets. Through this gap a cellulose-tri-acetate band is passed carrying weights attached to its lower end. This provides the accelerating force, and if it remains constant, the velocity of downward slip of the band is inversely proportional to the viscosity of the fluid. The latter is contained by a recess formed at the top of the blocks (Fig. 1).

The band is kept centred in the gap by the hydrodynamic pressure, but the energy dissipated in this way is so small that it can be neglected. Then:

$$K = 2.B.H.\frac{V}{A}\eta$$

where K is the force causing slip, B is the width of the band, H is the effective depth of the blocks, V is the speed of the downward slip, and A is the clearance between the surface of the band and the block.

A uniform temperature is maintained by circulating water in the blocks. The fluid between the blocks is continuously removed by the band and cannot cause additional heating, which would contribute to inaccuracy of measurements.

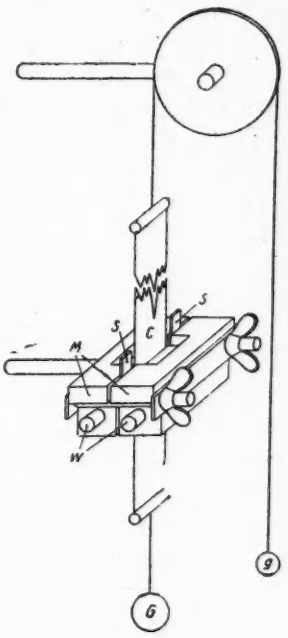


Fig. 1

M = Metal blocks S = Gaskets (150$\mu$) C = Cellulose-tri-acetate
W = Water pipes G = Accelerating force g = Counterweight

The viscosity of oils containing pigments in suspension was determined with this apparatus. The results were very interesting as they have revealed that, regardless of the viscosity of the oil, the curves obtained are identical, provided the viscosity extrapolated to $\infty$ shearing speed was plotted against the percentage pigment content. In other words, the pigment content alone determines the viscosity of the fluid, the kind of pigment in suspension being a modifying factor.

## TOUGHNESS OF MEDIUM-CARBON FORGING STEEL

(From *Technical News Bulletin*, No. 292, August 1941, p. 73).

SAMUEL J. ROSENBERG and Daniel H. Gagon have studied the relation between grain size and heat treatment and the impact-toughness of steel, particularly as affected by low temperatures. Most steels lose toughness (i.e., become brittle) quite rapidly as the temperature decreased. The range of temperature wherein this change occurs is a reliable criterion of the relative toughness of steels—the lower the temperature at which toughness is lost, the better the steel.

Six heats of the same type of medium-carbon forging steel, made so as to have different grain sizes, were studied. It was found that, as hot rolled, no relation existed between grain size and toughness, and all the steels were quite brittle. Normalizing (heating to 1600° F and air cooling) caused some improvement in toughness, and when so treated the fine-grained steels were tougher than the coarse-grained steels. Proper heat treatment (hardening and tempering) resulted in a marked improvement in the toughness of the steels, but in this condition there was no relation between grain size and toughness in the heat-treated steels.

The authors conclude that each individual heat of this type of steel has an inherent resistance to impact, characteristic of that particular heat, and that this impact resistance is dependent upon factors not at present recognised.

# stripped water

In the preparation of tobacco for good quality cigarettes, the centre stem is stripped from the leaf in the manner shown above, but if this process is not carried out, tobacco including the centre stalk is uneven and contains dust which irritates the throat of the smoker. Similarly with the water required for feeding into water tube boilers it is necessary to strip from it the soluble salts and other impurities in order to secure a non-scaling, non-corrosive feed water. The Permutit "Deminrolit" Process produces a perfect stripped water from any supply without the use of heat or steam.

*For full particulars write for publication "Distilled Water without Distillation" to The Permutit Company Limited, Dept. T.B., Permutit House, Gunnersbury Avenue, London, W.4. Telephone: Chiswick 6431.*